UNIVERSITY OF OKLAHOMA

GRADUATE COLLEGE

INTEGRATED PRODUCTION DATA ANALYSIS OF HORIZONTAL FRACTURED WELL IN UNCONVENTIONAL RESERVOIR

A THESIS

SUBMITTED TO THE GRADUATE FACULTY

in partial fulfillment of the requirements for the

Degree of

MASTER OF SCIENCE

By

DA ZHENG
Norman, Oklahoma
2016

INTEGRATED PRODUCTION DATA ANALYSIS OF HORIZONTAL FRACTURED WELL IN UNCONVENTIONAL RESERVOIR

A THESIS APPROVED FOR THE
MEWBOURNE SCHOOL OF PETROLEUM AND GEOLOGICAL ENGINEERING

BY

_____
Dr. Rouzbeh Ghanbarnezhad Moghanloo, Chair

_____
Dr. Zulfiquar Reza

_____
Dr. Siddharth Misra

Dedicate to my dear mom and dad who gave me countless love and support.

Acknowledgements

I would like to acknowledge my advisor, Dr. Rouzbeh Ghanbarnezhad Moghanloo – without his guidance and assistance, the process of conducting this research study, and indeed navigating my entire degree program, would have been exponentially more difficult. It is him that leading me to the new world of academy.

I also would like to acknowledge the committee members, Dr. Siddharth Misra and Dr. Zulfiquar Reza, for their guidance and support of my research.

I would like to acknowledge my girlfriend Jing Zhang. I also want to acknowledge my friend Bin Yuan and Kai Wang for their endless encouragement and support. Without their generous help, the research is not able to be completed successfully. I won't forget the countless nights we together dedicate in the research. I love you both!

Finally, I would like to thank my parents, Xingbo Zheng and Hongru Li. Throughout this entire process they helped me keep concentrate on the goal instead of small task. Their unfailing support and occasional criticism was exactly what I needed to accomplish my Master of Science degree at University of Oklahoma. Studying abroad for four years, I didn't perform enough duty as a child. Love you!

Table of Contents

List of Table

List of Figures

Abstract

This thesis presents a novel analytical solution to predict the expansion of drainage volume for compound transient linear flow system consisting of stimulated-reservoir volume (SRV) and unstimulated shale/tight sandstone matrix volume. The distance of investigation (DOI) has been demonstrated to be a useful notion for production data analysis; e.g., optimization of spacing of hydraulic fractures, and evaluation of stimulated-reservoir volume (SRV). The DOI concept has been mainly used to evaluate dynamic drainage volume (DDV) for the linear flow system only within SRV. Thus, in view of production from both SRV and unstimulated shale/tight sand matrix; the DOI (or DDV) of transient linear flow in compound multi-stage fractured reservoirs has not been able to be determined yet.

In this work, we derive the DDV equation analytically for compound transient linear flow system under constant-flowing-pressure and constant-production-rate condition for the compound linear flow system. To that end, coupled with the analytical equation calculating the pressure and DDV of linear flow within only SRV, the compound linear flow solution within both SRV and unstimulated matrix is derived. Laplace transform and numerical inversion are implemented to obtain the semi-analytical solution. The pressure front is calculated by implementing the impulse response concept, which is the maximum rate of pressure response. In addition, a relationship was established between DOI and square root of time using multivariable regression, based on the results of 2000 cases calculated from our semi-analytical solution. The cases capture the impact of several parameters, including different diffusivities within SRV and unstimulated matrix, hydraulic fracture length, and fracture spacing.

Our solution suggested that the DOI demonstrates a linear relationship to the square-root-of-time for both linear flow within SRV and the compound linear flow system. The advancement of DDV within stimulated-reservoir volume is significantly faster than that within unstimulated matrix. The majority of production is attributed to size of stimulated-reservoir volume. To verify the accuracy of the new DDV equations, we analyze the synthetic production data from a series of fine-grid numerical simulations.

Employing the DDV model and empirical equation, a novel workflow of integrated production data analysis is proposed to evaluate and predict the performance of multi-stage fractured horizontal well (MFHW). A weak (integral) form of macroscopic mass balance model with moving boundary is developed for the expanding productive region (drainage volume) during long-term transient-flow regimes in non-static shale reservoirs saturated with compressible fluids. The effects of stress-dependent reservoir and pressure-dependent fluid properties on production analysis are incorporated by a pressure-dependent correction factor. To verify the accuracy of our integrated analysis, firstly, we start with a synthetic simulation example with known parameters. In the next stages, several field examples are examined with our integrated analysis approach to evaluate and predict the performance of MFHW.

The size of DDV and associated average reservoir pressure, recovery factor (RF) and average saturation (oil/gas/water) are achieved. The half-length of primary fracture and diffusivity within SRV are also evaluated by coupled with a correction factor, and the ultimate drainage volume (estimated as ultimate recovery, EUR) is also predicated at abandonment condition, which indicates the maximum size of system affected by single-well production for us to optimize well spacing. Moreover, the contributions of both

unstimulated-reservoir matrix and stimulated-reservoir volume (SRV) are quantified with changing time, respectively.

The proposed approach has the following novel contributions: (1) capability to ascertain DDV and associated average reservoir pressure throughout different transient-flow regimes; (2) incorporating non-static, fluid compressibility, multi-phase flow and moving flow boundary effects into production history analysis; and 3) simplicity and efficiency; does not require comprehensive inputs as opposed to sophisticated numerical simulations, but could obtain almost all of the necessary parameters for evaluation and prediction.

Chapter 1: Introduction

This thesis presents work performed for a Master of Science degree that was conducted at Mewbourne School of Petroleum and Geological Engineering of the University of Oklahoma. The research presented herein develops an analytical model of dynamic drainage volume (DDV), describing a system of a multi-fracture horizontal well in a shale reservoir. Based on the DDV model, it also proposes an integrated production data analysis system to evaluate and predict the well. The following sections present the motivation behind the study as well as the objectives, background, approach and organization of the thesis.

1.1 Motivation and Problem Statement

Shales are the most abundant types of sedimentary rock all over the earth. They used to serve as a source rock for hydrocarbon and a seal rock for reservoir, which is able to generate and trap oil and gas. Recently, in North America, the advancement of the techniques of hydraulic fracturing and horizontal drilling made it possible to exploit low permeability gas and oil shale. Now, people all around world begin to find a specific type of shale - organic rich shale, which can act as a reservoir able to be produced.

Unconventional reservoirs refer to low or ultra-low permeability formation that can be exploited. Conventional reservoir means those ones with permeability bigger than 0.1mD, and unconventional reservoir means the ones having a permeability lower than 0.1mD. This is widely agreed by the industry, even though there is no scientific basis behind it.

To produce the shale gas/oil effectively, people need to stimulate the formation near wellbore and maximize the contact area available to flow. Consequently, horizontal

drilling and hydraulic fracturing are widely employed to produce the shale reservoir. A horizontal well could be drilled for thousands of feet length. The reservoir situation around the well is more complicated than conventional reservoirs. So, this needs a more complex model to describe the fluid flow compared for the conventional reservoir; and based on this model, some analysis method should be proposed to analyze the stimulation and reservoir property accurately.

Some investigators proposed different methods to perform the production data analysis (PDA) for shale/tight sandstone reservoir. Rate transient analysis, like pressure transient analysis) is a relatively new method of PDA, where production rate and flowing pressure are used to estimate reservoir properties (i.e. fracture length, matrix permeability, hydrocarbon in place and so on). Rate transient analysis method is not fully developed for unconventional reservoirs, some of the authors do not consider the fluid property change incurred by pressure drop; some of them ignore the reservoir properties change while producing; and they also disregard the production contribution of outer reservoir.

For this purpose, this thesis aims to propose an integrated system to analyze production data, which can evaluate the properties of the reservoir and predict the future production condition.

1.2 Objective

(1) Develop an analytical solution for dynamic drainage volume (DDV), considering the production contribution from both inner reservoir (stimulated reservoir volume) and outer reservoir (unstimulated reservoir volume).

(2) Develop an integrated production data analysis system, which can evaluate the reservoir and stimulation properties based on production data history and able to predict future production condition.

(3) Apply the method derived before to analyze 10 multi-fractured horizontal wells, and perform the prediction and analysis.

1.3 Organization of Thesis

Chapter 2 is literature review, which provides the former study of investigation of radius, flow model of multi-fractured horizontal well, and production data analysis.

Chapter 3 derives the analytical solution for tri-linear flow model, considering the flow of both inner reservoir (stimulated reservoir volume) and outer reservoir (unstimulated reservoir volume). Based on the analytical solution, the dynamic drainage volume (DDV) propagated within outer reservoir has been quantified, with the maximum response method. Since the equation is complicated, multi-variable regression method is used to simplify into an empirical equation, coupling the variables inner diffusivity, outer diffusivity, fracture half-length and fracture spacing. Verification against the result of simulation software CMG is provided, and the result presents a good match. According to the DDV model and empirical equation derived before, fracture spacing optimization is performed.

Chapter 4 proposes a novel production analysis system. Macroscopic compressibility tank model is proposed to capture the average pressure and average saturation for a reservoir with moving flow boundary. Since the parameter of gas and oil are pressure related, pseudo variables and correction factor are introduced to capture the flow regime. Rate normalized pseudo-pressure analysis method is proposed to eliminate

the effect of various well operation and pressure dependent variables. Finding the fracture half-length with iterative calculation, coupled the skills mentioned above to build the integrated production system. Model validation is performed to assure the accuracy of the production data analysis procedure.

Chapter 5 is dedicated to field case application. Evaluating the production history, 10 oil production horizontal wells from the same reservoir are analyzed based on the method developed before. With decline curve analysis, the ultimate recovery factor, abandonment DDV and abandonment pressure are evaluated. It also provides the IPR calculation and analysis for that 10 wells and conclude the relationship between.

Chapter 6 is the conclusion of this thesis, including the contribution and progress with respect to this research area.

Chapter 2: Literature Review

This thesis consists of two major part, the first deals with dynamic drainage volume and the second deals with production data analysis of multi-fractured horizontal well in unconventional formation (gas/oil shale, tight gas sandstone). The following literature review covers studies related to these two topics.

The propose of developing an analytical model for a complex system is to make the problem simple. The complex system stated here is the area around multi-fractured horizontal well, including fracture, stimulated reservoir volume (inner reservoir) and unstimulated reservoir volume (outer reservoir), within an unconventional reservoir.

Carslaw and Jaeger (1959) proposed the analytical solution and the solution techniques for three-dimensional continuous conduction problems. This solution technique was introduced to the application of fluid flow in porous media afterwards, which includes the well-known methods source and sink, Laplace transformation, and Green's function. Van Everdingen and Hurst (1949) first employed Laplace transformation into the solution of diffusion equation of single phase fluid flow in porous media. Sometimes, the solution in Laplace domain is still complicated to perform analytical inversion, so numerical inversion is proposed by Stehfest (1970). Comparing with the other numerical inversion method presented afterwards, the method proposed by Stefest is still the most popular one for fluid flow in porous media.

The tri-linear flow model was first introduced by Lee and Brockenbrough (1986) to study the transient flow behavior of a well intercepted by a finite-conductivity vertical fracture. For both constant bottom-hole pressure and constant production rate, the solutions are provided. The model is shown in Fig. 2.1 and Fig. 2.2. The reservoir

surrounding a fracture has been divided into three regions, region 1, 2 and 3. The purpose the author separates region 2 and 3 is to make the boundary condition of diffusion equation convenient. Region 1 is fracture, whose flow is dominated in x-direction; because the ratio of fracture length to width is high. Region 2 is controlled by y-axis flow and region 3 is controlled by x-axis flow.

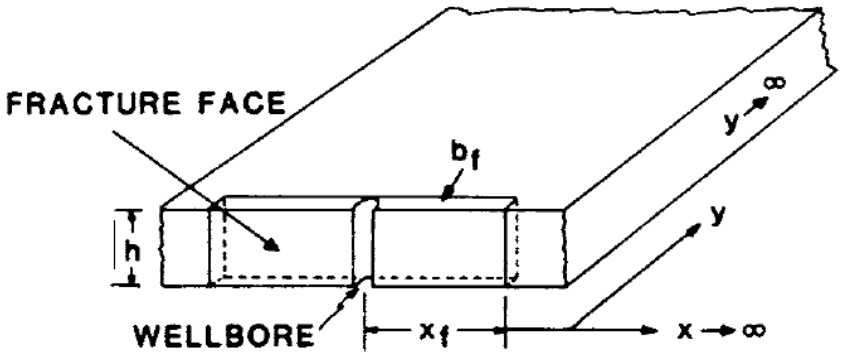

Figure 2.1 Infinite reservoir with a vertical fracture (Lee and Brockenbrough, 1986)

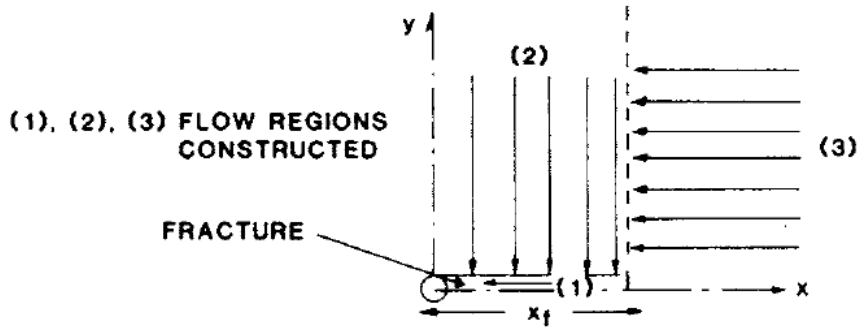

Figure 2.2 A quadrant of the top view of the fractured well system and trilinear flow approximation (Lee and Brockenbrough, 1986)

Brown et al. (2011) employs this tri-linear model in multi-fractured horizontal well within shale reservoir, which has ultra-low matrix permeability. It presents an analytical solution for the model that incorporates fluid flow from outer reservoir to inner reservoir, and final converge into fracture.

So far, a variety of authors have developed different concepts or models to estimate the distance of investigation, and for defining the stabilization time (time reaching pseudo-steady or steady state). For example, Tek et al. (1957) proposed the drainage radius at that point where the fluid flowing is 1% of the fluid flowing into the wellbore. Jones (1962) defined the drainage radius as the distance at which the pressure changes only by 1%. H.K. van Poollen (1964) equated the Y function of infinite and finite reservoirs that allows calculating the radius of investigation. Aguilera (1987) extended van Poollen's equation to the case of naturally fractured reservoirs that are represented by dual porosity systems. Sobbi and Badakhshan (1996) and Aguilera (2006) published a radius of investigation equation for well test analysis with pseudo-steady state inter-porosity flow for both dual-porosity finite and infinite reservoirs. Wattenbarger et al. (1998) proposed a new equation of DOI by indicating the end of the half-slope line in type curves. Kuchuk (2009) presented a comprehensive study on the DOI for radial flow. However, the dominate flow for multi-stage fractured horizontal wells in ultra-tight or shale reservoirs is the transient linear flow, which can last for several years. In addition to some empirical models for DOI, only within the SRV has an analytical formulation of DOI been recently employed to evaluate the dynamic drainage volume (DDV) for the linear flow system. Behmanesh et al. (2015) applied two different approaches to calculate the DOI, which are the maximum rate of pressure response method, and the transient-boundary flow intersection method. However, in view of production from both SRV and unstimulated shale/tight sand matrix, the DOI (or DDV in view of volume) of transient linear flow in compound multi-stage fractured reservoirs has not been determined yet. Moghanloo et al. (2015) proposed an empirical equation of DDV based on its

asymptotical relation with production time. Nobakht and Clarkson (2012) ignored the production contribution outside the stimulated-reservoir volume (SRV); therefore, it is assumed that there is only transient linear flow within SRV. However, as the assumption of the trilinear flow model from Brown et al. (2011), and the continuing production of multi-stage fractured horizontal well after linear flow, there would be a compound linear flow (Song and Ehilg-Economides, 2011) regime, where both SRV and unstimulated reservoirs near SRV can contribute fluid productions.

Typically, it is critical to make accurate reservoir/fracture characterization and well performance prediction for the economic development of unconventional reservoirs. Reservoir evaluation techniques, based on core samples, well logs, and pressure and rate transient data analysis, have been developed rapidly to help evaluate formation and fracture network properties (Clarkson et al., 2012; Osholake, et al., 2012). In shale reservoirs, a wide range of complex reservoir/fluid properties (i.e., gas desorption, non-Darcy, and multi-phase flow; ultra-low permeability, stress-dependent porosity, and dual-porosity/dual-permeability etc.) and macro/micro fracture network distribution lead to conventional evaluation methods that are not accurate enough. The objectives of production data analysis (PDA) are to obtain: (1) reservoir and well stimulation characterization, (2) evaluation of dynamic drainage efficiency, and (3) forecast of reservoir performance and development planning (Yuan B., et al., 2015). As discussed by Clarkson and Beierle (2011), there are several production analysis techniques commonly used in unconventional reservoirs, including straight-line analysis, type-curve methods, analytical/numerical solutions and empirical methods. Type-curve methods consist of matching the production history to dimensionless solutions, which correspond

to different well/fracture geometries, reservoir types and boundary conditions (Yin J., et al., 2011; Lee J., et al., 2003 and Wang L., et al., 2013). Straight-line analysis methods illustrate the typical flow regimes with the use of derivative analysis or log-log diagnostic techniques. It can help in extracting well geometry, fracture and reservoir properties and well productivity during different flow regimes: linear or bilinear flow (fracture half-length and fracture conductivity), elliptical flow (reservoir permeability and fracture length), radial flow regime (skin and reservoir permeability), and boundary-dominated flow (OGIP and flow coefficient) (Clarkson et al., 2011; Cheng Y., et al., 2009). Decline models used include Arps decline-curve methodology (Asps J., 1945), "power-law exponential" (Ilk D., et al., 2008) and "stretched-exponential" (Valko P., et al., 2010), which can consider the long-term transient and transitional flow in tight and shale gas reservoirs. Duong method (Duong, 2010) and modified Duong method (Joshi, 2012) provided a new forecasting model based on the long-term linear flow regime. Variety of numerical simulation and analytical models have been extensively presented by (Seidle 1999, Javadpour 2009, Cipolla, Lolon et al. 2010, Ozkan, Raghavan et al. 2010, Apaydin, Ozkan et al. 2012, Swami and Settari 2012, Yuan et al. 2015), and their models consider different complex characteristics of shale or tight reservoirs, such as desorption of gas, non-Darcy flow effects, complex hydraulic fractures and micro fractures. Despite those diverse methods to evaluate and simulate shale reservoirs with on-going development, these models always require extensive computation and require knowledge of reservoir properties that may not always be known, such as the average reservoir pressure and fracture/reservoir properties at any time. Moreover, at early stage of production, there are usually not enough data for us to characterize the heterogeneous fracture/reservoir

properties in unconventional reservoir, hence, the more detailed and complicated numerical simulation or simplified analytical solutions may not be a viable option to evaluate and predict reservoir performance efficiently.

The dominated flow regime for multi-fractured horizontal wells (MFHW) in tight/shale formations is transient linear flow, which can continue for several years. Rate-normalized pressure analysis with material balance time is commonly used to interpret flow regimes. However, for stress-sensitive reservoirs with compressible fluids, the mass balance pseudo-time should be adopted to couple the effects of changing reservoir pressure on fluid and reservoir properties (Anderson and Mattar, 2007). The square-root-of-time plot during transient linear flow regimes as a popular method can be used to evaluate properties of fractures/stimulated-reservoir volume. However, if the fluid/reservoir pressure-dependent properties cannot be accounted into pseudo-variables, the interpretation results of square-root-of-time may result in incorrect evaluation of fracture/reservoir properties. Nobakht and Clarkson (2012), and H. Behmanesh et al., (2015) have corrected the pseudo-time definition coupled with changes of average reservoir pressure, and presented analysis for both constant-FBHP production and constant-rate production cases. Therefore, it is an essential step to predict the changes of average reservoir pressure for variable FBHP and production rates cases, which in turn affect the reservoir (pressure-dependent permeability/porosity) and fluid (compressible gas or slight compressible oil) properties. One of the objectives in this paper is to improve the calculation of average reservoir pressure within dynamic drainage volume by considering those pressure-dependent effects, for the purpose of more accurate

production data analysis during long-term transient-linear flow regimes in unconventional reservoirs.

Moghanloo et al. (2015), Yuan et al (2016) and Clarkson et al. (2015) studied the concept of dynamic drainage volume (DDV) during long-term transient linear flow regimes in unconventional reservoirs. Estimation of DDV is another important objective of production data analysis. As noted, the primary production in ultra-low/shale reservoirs is attributed to the stimulated-reservoir volume (referred to dynamic drainage volume corresponding to the end of transient-linear flow). Although the stimulated-reservoir volume can also be roughly calculated from micro-seismic mapping, it also needs to be tuned by analytical and numerical solutions and production data analysis. Zheng et al (2016) derived an analytical-empirical equation of DDV by using the maximum rate of pressure response and multi-variable regression method, which is applicable for the compound linear flow across both the inner stimulated-reservoir volume and outer unstimulated matrix. This paper will introduce this novel formula of DDV into macroscopic model to evaluate the dynamic change of average pressure within DDV. In addition, transient-productivity index analysis provides a useful tool to characterize the decline of production performance (F. Medeiros et al., 2010). In shale reservoirs, matching transient-production index with multiple flow regimes can improve the accuracy of transient rate-decline analysis. In addition, as noted, the production index is usually used to characterize productivity potential of fractured horizontal well, i.e., the increase of production index can indicate the improvement of fracturing stimulation efficiency in unconventional reservoirs.

Chapter 3: Modeling Dynamic Drainage Volume for Multi-Stage Horizontal Well

3.1 Multi-stage Fractured Horizontal Well Flow Model Derivation

3.1.1 Assumption

The tri-linear flow model proposed by Brown (2011) is specifically applicable to a multi-stage fractured horizontal well (MFHW) in an unconventional reservoir with ultra-low matrix permeability. In order to get the analytical solution for this model, several assumptions have been made based on the character of unconventional reservoir.

The foundation of this flow model is the premise that linear flow regime is dominant in both stimulated reservoir volume (SRV) and unstimulated reservoir volume for a long time while producing from a MFHW. The model then divides the reservoir into three regions, hydraulic fracture, inner reservoir (stimulated reservoir volume) and outer reservoir (unstimulated reservoir volume). As shown in Fig. 3.1, the outer reservoir is the region beyond the tips of fractures, the inner reservoir is the region between two adjacent fractures, and the hydraulic fracture itself. For the following equations, we use subscript "I" to represent the inner reservoir, "O" to represent the outer reservoir, and "F" to represent the fracture region. The properties of each region are different.

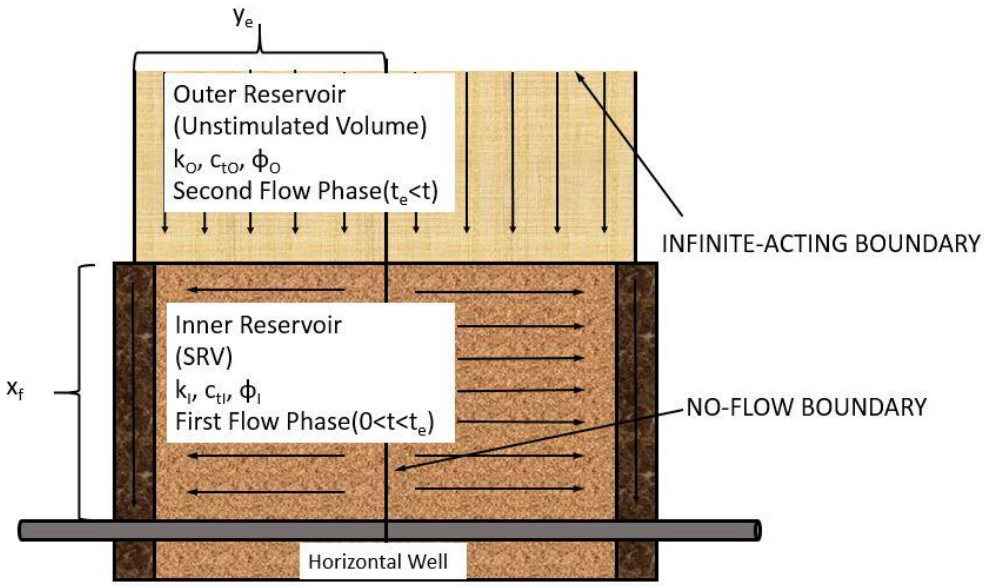

Figure 3.1 Schematic picture of tri-linear flow model for multi-fractured horizontal well

This thesis assumes that along the horizontal well, each fracture has the identical properties and equally fracture spacing. the transient flow response of many identical transverse hydraulic fractures of a horizontal well can be modeled via considering a single fracture and the rectangular area around it (Fig. 3.2). This assumption is a common field practice and able to provide enough accurate solutions. The total production rate of the horizontal well is the accumulation of the production of each single symmetric fracture. Similarly, as sketched in Fig.3.1 and 3.2, the total DDV of the horizontal well is the DDV summation of each identical symmetry element. Our analytical solution is derived from considering one-quarter of a hydraulic fracture and its corresponding DDV.

It assumes that as soon as the DDV arrived mid-line between two adjacent fractures, which is the no-flow boundary of the inner reservoir, the outer reservoir just starts to flow into the inner reservoir as another linear flow system. The reason we make this assumption is that the purpose of this mathematic model is to capture the distance of investigation (DOI) within outer reservoir and inner reservoir separately, so the

production contribution of outer reservoir cannot mix with the production of inner reservoir at the first flow phase. Since the permeability of SRV is bigger than 10 times of outer reservoir, then outer reservoir production contribution is minute comparing with the production contribution of inner reservoir during first flow phase, it is a reasonable assumption.

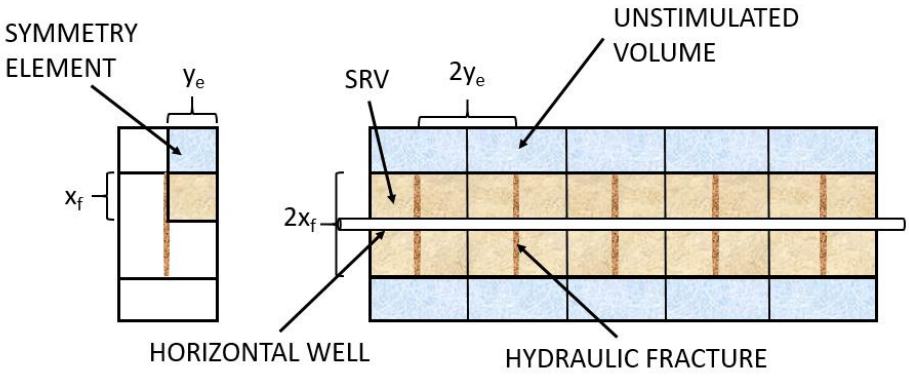

Figure 3.2 MFHW and symmetry element employed to derive the mathematical model

During the production, it assumes that the absolute permeability is constant, and the capillary effect and gravitational force are neglected. There is no skin factor nor well storage effect.

In this work, we regard the conductivity of hydraulic fracture as infinite, which means it has the same pressure as flowing pressure. For convenience, we derive the analytical solution for this tri-linear model in dimensionless variables. The definition is presented in section 3.1.2 and the derivation of the flow model is presented in section 3.1.3.

3.1.2 Dimensionless variable definition

The flow model is derived in dimensionless variables for convenience, and in SI units constantly. The definition of dimensionless variables is described here.

Dimensionless pressure is defined as:

$$p_D = \frac{2\pi k_I h}{qB\mu}\left(p_i - p\right) \quad \text{(3.1)}$$

Dimensionless time is defined as:

$$t_D = \frac{\eta_I t}{x_F^2} \quad \text{(3.2)}$$

Diffusivity of inner and outer reservoir are defined separately as:

$$\eta_I = \frac{k_I}{\left(\phi C_t\right)_I \mu} \quad \text{(3.3)}$$

$$\eta_O = \frac{k_O}{\left(\phi C_t\right)_O \mu} \quad \text{(3.4)}$$

Dimensionless distances in x and y directions are defined as:

$$y_D = \frac{y}{x_F} \quad \text{(3.5)}$$

$$x_D = \frac{x}{x_F} \quad \text{(3.6)}$$

The dimensionless diffusivity based on inner and outer reservoir are defined as:

$$\eta_{OD} = \frac{\eta_O}{\eta_I} \quad \text{(3.8)}$$

Dimensionless reservoir conductivity is defined as:

$$C_{RD} = \frac{k_I x_F}{k_O y_e} \quad \text{(3.9)}$$

3.1.3 Derivation of Analytical Solution

In this section, the derivation of the solution of tri-linear flow model is presented. Because of the equality of each fracture as assumption, the solution is calculated based on a quarter of a hydraulic fracture region as shown in Fig. 3.2. At first, the solution is derived with respect to outer reservoir and inner reservoir separately. Then the solutions are coupled by pressure continuity and flux continuity between two regions as boundary conditions. The solution is derived in Laplace domain and numerical inversion method proposed by Stehfest (1970) is used to get the solution in real time domain.

The governing equation of fluid flow in porous media is diffusion equation, which is derived by mass balance equation and Darcy's Law. The equation of single phase fluid flow of a constant compressibility and in homogeneous and anisotropy porous media is,

$$k_x \frac{\partial^2 p}{\partial x^2} + k_y \frac{\partial^2 p}{\partial y^2} + k_z \frac{\partial^2 p}{\partial z^2} = \phi \mu c_t \frac{\partial p}{\partial t} \quad \text{.....(3.10)}$$

The first step to calculate the tri-linear flow model is deriving the outer reservoir solution, which can be started from Eq. 3.10,

$$k_O \nabla^2 p_o = \phi_O c_{tO} \mu \frac{\partial p_O}{\partial t} \quad \text{.....(3.11)}$$

The subscript 'O' represent parameters of outer reservoir. Since flow from outer reservoir into inner reservoir can be assumed linear, demonstrated in Fig.3.1, the Eq. 3.11 can be written as

$$k_O \frac{\partial^2 \Delta p_O}{\partial x^2} = \phi_O c_{tO} \mu \frac{\partial p_O}{\partial t} \quad \text{.....(3.12)}$$

With the definition of 3.1.2, the dimensionless form of Eq. 3.12 is

$$\frac{\partial^2 p_{OD}}{\partial x_D^2} - \frac{1}{\eta_{OD}} \frac{\partial p_{OD}}{\partial t_D} = 0 \quad \text{.....(3.13)}$$

Applying Laplace transformation,

$$\frac{\partial^2 \bar{p}_{OD}}{\partial x_D^2} - s_o \bar{p}_{OD} = 0$$

… . (3 . 1 4)

$$s_O = \frac{s}{\eta_{OD}} \quad \text{.........(3.15)}$$

The overbar symbol represents dimensionless pressure of the outer reservoir in the Laplace-transform domain, and is the Laplace parameter with respect to dimensionless time, t_D. The general solution for this is,

$$\bar{p}_{OD} = A\exp(-\sqrt{s_O}\, x_D) + B\exp(\sqrt{s_O}\, x_D) \quad \text{.........(3.16)}$$

In practical, for most of production wells the effect of flowing boundary of outer reservoir cannot be felt during production life because of ultra-low matrix permeability. The effect of other wells is not considered in this flow model, then for the transient flow state, the outer boundary conditions are described as,

$$\bar{p}_{OD} = 0 \text{ at } x \to +\infty \quad \text{.........(3.17)}$$

Substitute the Eq. 3.17 into Eq. 3.16, solving for B,

$$B = 0 \quad \text{.........(3.18)}$$

Hence, the transient pressure solution for outer reservoir is,

$$\bar{p}_{OD} = \left(\bar{p}_{ID}\right)_{x_D=1} \exp\left(\sqrt{s_o}\left(1 - x_D\right)\right) \quad \text{.........(3.19)}$$

For the contact surface between inner reservoir and outer reservoir, the pressure must be equal,

$$\left(p_{OD}\right)_{x_D=1}=\left(p_{ID}\right)_{x_D=1} \text{ at } x_D=1 \quad \text{.....(3.20)}$$

With Eq. 3.19 and 3.20, the value of A can be solved,

$$A=\frac{(\overline{P}_{ID})_{x_D=1}}{\exp(-\sqrt{s_o})} \quad \text{.....(3.21)}$$

Hence, the transient pressure solution for outer reservoir is,

$$\bar{p}_{OD}=\left(\bar{p}_{ID}\right)_{x_D=1}\exp\left(\sqrt{s_o}\left(1-x_D\right)\right) \quad \text{..... (3.22)}$$

Eq. 3.19 is the solution for outer reservoir in Laplace domain, which is left for coupling with the inner reservoir solution by pressure continuity at contact surface. The properties of outer reservoir are included in Eq. 3.8.

The next step of deriving of trilinear flow model solution is to calculate the inner reservoir solution, which can be started from Eq. 3.10,

$$k_I\nabla^2 p_I=\phi_I c_{tI}\mu\frac{\partial p_I}{\partial t}, \quad \text{.....(3.23)}$$

Noting that the subscript ‘I’ denotes parameters of inner reservoir. As presented in Fig.3.1, for the inner reservoir, assuming the fluid flow from the outer reservoir into the inner reservoir is along the x direction; meanwhile, the fluid flow from inner reservoir into the primary fracture is along y direction, the governing equation can be expressed in two dimensions,

$$\frac{\partial^2\Delta p_I}{\partial x^2}+\frac{\partial^2\Delta p_I}{\partial y^2}=\frac{\phi_I c_{tI}\mu}{k_I}\frac{\partial p_I}{\partial t} \quad \text{.....(3.24)}$$

Integrating both sides of Eq.3.24,

$$\int_0^{x_F} \frac{\partial^2 \Delta p_I}{\partial x^2} \partial x + \int_0^{x_F} \frac{\partial^2 \Delta p_I}{\partial y^2} \partial x = \frac{\phi_I c_{tI} \mu}{k_I} \int_0^{x_F} \frac{\partial \Delta p_I}{\partial t} \partial x \quad \text{..... (3.25)}$$

Because of the assumption,

$$\frac{\partial p_I}{\partial y} \neq f(x) \quad \text{.....(3.26)}$$

$$\frac{\partial p_I}{\partial t} \neq f(x) \quad \text{.....(3.27)}$$

and $\left(\frac{\partial \Delta p_I}{\partial x} \right)_{x=x_F} = \left(\frac{\partial \Delta p_O}{\partial x} \right)_{x=x_F}$, ...(3.28)

the equation (3.25) can be simplified to:

$$\frac{\partial^2 \Delta p_I}{\partial y^2} + \left(\frac{k_o}{k_I k_F} \right) \left(\frac{\partial \Delta p_O}{\partial x} \right)_{x=x_F} = \frac{\phi_I c_{tI} \mu}{k_I} \frac{\partial p_I}{\partial t} \quad \text{.....(3.29)}$$

Converting Eq. 3.29 into dimensionless form with the definition in section 3.2, it becomes

$$\frac{\partial^2 \Delta p_{ID}}{\partial y_D^{\,2}} + \left(\frac{k_o x_F}{k_I k_F} \right) \left(\frac{\partial \Delta p_{OD}}{\partial x_D} \right)_{x_D=1} = \frac{\partial p_{ID}}{\partial t_D} \quad \text{.....(3.30)}$$

The reason of defining the dimensionless reservoir conductivity, C_{RD} , is that relating flow within inner reservoir to flow within outer reservoir. Then, the fracture half spacing, y_e, is included in the Eq. 3.9,

$$\frac{\partial^2 \Delta p_{ID}}{\partial y_D^{\,2}} + \left(\frac{k_o x_F}{k_I k_F} \right) \left(\frac{y_e}{y_e} \right) \left(\frac{\partial \Delta p_{OD}}{\partial x_D} \right)_{x_D=1} = \frac{\partial p_{ID}}{\partial t_D} \quad \text{.....(3.31)}$$

Rearranging the equation,

$$\frac{\partial^2 \Delta p_{ID}}{\partial y_D{}^2} + \left(\frac{1}{y_{eD}}\right)\left(\frac{\partial \Delta p_{OD}}{\partial x_D}\right)_{x_D=1} - \frac{\partial p_{ID}}{\partial t_D} = 0 \quad \text{.....(3.32)}$$

Employing Laplace transformation,

$$\frac{\partial^2 \bar{p}_{ID}}{\partial y_D{}^2} + \left(\frac{1}{y_{eD}}\right)\left(\frac{\partial \bar{p}_{OD}}{\partial x_D}\right)_{x_D=1} - s\bar{p}_{ID} = 0 \quad \text{..... (3.33)}$$

$$\frac{d^2 p_{ID}}{dy_D^2} - \alpha p_{ID} + p_{ID}\left(t_D = 0\right) = 0 \quad \text{.....(3.34)}$$

Where

$$\alpha = \frac{\sqrt{s_O}}{C_{RD} y_{eD}} + s \quad \text{.....(3.35)}$$

3.1.4 Constant-FBHP Boundary

As described in the section 3.1.1, for the reason that the difference of permeability between SRV and unstimulated volume is significant, it is reasonable to assume that fluid of outer reservoir starts to flow into inner reservoir as soon as the distance of investigation (DOI) arrived the mid-line between two fractures. Instead of setting the time the well starts to produce as 0, the time when fluid starts to flow from outer reservoir into inner reservoir is set as 0 for the derivation. It is because that the propose of this derivation is to capture the expansion of DDV within outer reservoir with respect to time. As a consequence, the initial condition for the inner fractured reservoir are listed as follows (Behmanesh. et al. 2015):

$$p_{ID}\left(t_D = 0\right) = erfc\left(\frac{y_D}{2\sqrt{t_{eD}}}\right), \text{ at } 0 < y_D < y_{eD},\ t_D = 0 \quad \text{.....(3.36)}$$

The dimensionless time needed for DOI arriving the mid-line of two hydraulic fractures is:

$$y_{eD} = \sqrt{6t_{eD}} \quad \text{.....(3.37)}$$

The no-flow boundary condition in the middle of the two adjacent fractures is:

$$\frac{dp_{ID}}{dy_D} = 0, \text{ at } y_D = y_{eD}, t_D > 0 \quad \text{.....(3.38)}$$

The boundary condition at the interface of hydraulic fracture:

$$p = p_{wf} \rightarrow p_D = 1, \text{ at } y_D = 0 \quad \text{..... (3.39)}$$

The solution for the non-homogeneous partial-differential equation with the preceding initial and boundary conditions is composed by the part of general solution and the part of a particular solution, as follows:

$$p_{ID} = C_1 \exp\left(\sqrt{\alpha} y_D\right) + C_2 \exp\left(-\sqrt{\alpha} y_D\right) + b_5 y_D^5 + b_4 y_D^4 + b_3 y_D^3 + b_2 y_D^2 + b_1 y_D^1 + b_0 \quad \text{.....(3.40)}$$

Where,

$$b_5 = -\frac{9\sqrt{6}}{40\sqrt{\pi} y_{eD}^5} \quad \text{.....(3.41)}$$

$$b_4 = \frac{1}{\alpha} \quad \text{.....(3.42)}$$

$$b_3 = -\frac{\sqrt{6}}{\alpha\sqrt{\pi} y_{eD}} + \frac{3\sqrt{6}}{2\alpha^2\sqrt{\pi} y_{eD}^3} - \frac{27\sqrt{6}}{\alpha^3\sqrt{\pi} y_{eD}^5} \quad \text{.....(3.43)}$$

$$b_2 = 0 \quad \text{.....(3.44)}$$

$$b_1 = \frac{\sqrt{6}}{2\alpha y_{eD}^3 \sqrt{\pi}} - \frac{9\sqrt{6}}{2\alpha^2 \sqrt{\pi} y_{eD}^5} \quad \text{.....(3.45)}$$

$$b_0 = 0 \quad \text{.....(3.46)}$$

$$C_1 = \frac{1}{\sqrt{\alpha}\exp\left(\sqrt{\alpha} y_{eD}\right) + \sqrt{\alpha}\exp\left(-\sqrt{\alpha} y_{eD}\right)} \times$$

$$\left[\left(1-b_0\right)\exp(-\sqrt{\alpha} y_{eD}) - 5b_5 y_D^4 + 4b_4 y_D^3 + 3b_3 y_D^2 + 2b_2 y_D^1 + b_1\right] \quad \text{.....(3.47)}$$

$$C_2 = 1 - b_0 - C_1 \quad \text{.....(3.48)}$$

Followed by, the dimensionless pressure for the outer reservoir in Laplace-transform domain is:

$$\bar{p}_{OD} = \left(C_1 \exp\left(\sqrt{\alpha} y_D\right) + C_2 \exp\left(-\sqrt{\alpha} y_D\right) + b_5 y_D^5 + b_4 y_D^4 + b_3 y_D^3 + b_2 y_D^2 + b_1 y_D^1 + b_0\right)$$

$$\exp\left(\sqrt{\frac{s}{\eta_{OD}}}\left(1 - x_D\right)\right) \quad \text{.....(3.49)}$$

3.1.5 Constant-Rate Boundary Condition

For the case with constant production rate, it also assumes that the outer reservoir starts to flow when the DOI of the inner reservoir arrives at the mid-line of two fractures. Meanwhile, similar with the constant-pressure condition, we regard the time when the outer reservoir starts to flow as initial condition, $t_D = 0$. So the initial condition for inner reservoir is listed as follows (Behmanesh. et al. 2015):

$$P_{ID}(\mathrm{t}_D = 0) = \pi\left[2\sqrt{\frac{t_D}{\pi}}\exp\left(-\frac{y_D}{4t_{eD}}\right) - y_D erfc\left(\frac{y_D}{2\sqrt{t_{eD}}}\right)\right], \text{ at } 0 < y_D < y_{eD}\ , t_D = 0 \quad \text{.....(3.50)}$$

Then applying the theory of maximum pressure response (Behmanesh. et al. 2015), the dimensionless time needed for DOI arriving the mid-line of two hydraulic fractures is:

$$y_{eD} = \sqrt{2t_{eD}} \quad \text{(3.51)}$$

The boundary conditions are described as:

$$\frac{dP_{ID}}{dy_D} = -\pi \text{ , at } y_D = 0 \text{ , } t_D > 0 \quad \text{(3.52)}$$

$$\frac{dp_{ID}}{dy_D} = 0 \text{ , at } y_D = y_{eD} \text{ , } t_D > 0 \quad \text{(3.53)}$$

The solution for the non-homogeneous partial-differential equation (Eq.10) with preceding initial and boundary conditions is:

$$\bar{p}_{ID} = C_1 \exp\left(\sqrt{\alpha} y_D\right) + C_2 \exp\left(-\sqrt{\alpha} y_D\right) + b_6 y_D^6 + b_5 y_D^5 + b_4 y_D^4 + b_3 y_D^3 + b_2 y_D^2 + b_1 y_D^1 + b_0 \quad \text{(3.54)}$$

Where

$$b_6 = \frac{\sqrt{\pi}}{120\sqrt{2}\alpha y_{eD}^5} \quad \text{(3.55)}$$

$$b_5 = 0 \quad \text{(3.56)}$$

$$b_4 = \frac{\sqrt{\pi}}{4\sqrt{2}\alpha^2 y_{eD}^5} - \frac{\sqrt{\pi}}{12\sqrt{2}\alpha y_{eD}^3} \quad \text{(3.57)}$$

$$b_3 = 0 \quad \text{(3.58)}$$

$$b_2 = \frac{3\sqrt{\pi}}{\sqrt{2}\alpha^3 y_{eD}^5} - \frac{\sqrt{\pi}}{\sqrt{2}\alpha^2 y_{eD}^3} + \frac{\sqrt{\pi}}{\sqrt{2}\alpha y_{eD}} \quad \text{(3.59)}$$

$$b_1 = -\frac{\pi}{\alpha} \quad \text{.....(3.60)}$$

$$b_0 = \frac{6\sqrt{\pi}}{\sqrt{2}\alpha^4 y_{eD}^5} - \frac{\sqrt{2\pi}}{\alpha^3 y_{eD}^3} + \frac{\sqrt{2\pi}}{\alpha^2 y_{eD}^2} + \frac{\sqrt{2\pi}}{\alpha} y_{eD} \quad \text{.....(3.61)}$$

$$C_1 = \frac{1}{\sqrt{\alpha}\exp(\sqrt{\alpha} y_{eD}) - \sqrt{\alpha}\exp(-\sqrt{\alpha} y_{eD})} \left(\begin{array}{l} \left(p_i + b_1\right)\exp\left(-\sqrt{\alpha} y_{eD}\right) - \\ \left(6b_6 y_D^5 + 5b_5 y_D^4 + 4b_4 y_D^3 + 3b_3 y_D^2 + 2b_2 y_D + b_1\right) \end{array} \right)$$

.....(3.62)

$$C_2 = \frac{\pi + b_1 + C_1\sqrt{\alpha}}{\sqrt{\alpha}} \quad \text{.....(3.63)}$$

Then, the dimensionless pressure for the outer reservoir in Laplace-transform domain at any time is:

$$\bar{p}_{OD} = \left(C_1 \exp\left(\sqrt{\alpha} y_D\right) + C_2 \exp\left(-\sqrt{\alpha} y_D\right) + b_6 y_D^6 + b_5 y_D^5 + b_4 y_D^4 + b_3 y_D^3 + b_2 y_D^2 + b_1 y_D^1 + b_0\right)$$

$$\exp\left(\sqrt{\frac{s}{\eta_{OD}}}\left(1 - x_D\right)\right) \quad \text{.....(3.64)}$$

3.2 Determination of Dynamic Drainage Volume (DDV)

For the first flow phase, it assumes that only the fluid within inner reservoir contribute to the production. The analytical solution of DDV representing transient linear flow within only SRV has been proposed, Eq. 3.27. After the transient flow has reached the mid-line of inner reservoirs (Fig. 3.1 and Fig. 3.2), the DDV will propagate into the outer reservoirs. The equation calculating the DDV of a single fracture within outer reservoir can be calculated by,

$$DDV(\textit{within outer reservoir}) = DDV \text{ of inner reservoir} +$$

$$DOI(\textit{within outer reservoir}) \times \textit{fractureSpacing} \times \textit{thickness} \quad \text{.....(3.65)}$$

The value of distance of investigation (DOI) is required in this equation. The concept of DOI has been widely accepted for many years in well testing analysis to dictate the propagation of a pressure transient away from a wellbore that start to feel pressure disturbance (Lee et al. 2003). In other words, it is a concept used in well testing to measure how fast pressure waves propagate through reservoirs.

The method calculating DOI is not unique. Different authors gave different definitions of DOI, and Kuchuk (2009) provide a study of various definitions of DOI for radial geometry. The most widely used definition for DOI is the calculated maximum distance in a formation where pressure has been influenced during transient flow period. Many investigators employ the time at which a pseudosteady-state pressure distribution is attained in a closed circular area. Some other authors regard the distance at which the pressure drop reaches 1% of the pressure drop of wellbore as DOI.

Based on the theoretical basis, the DOI of linear flow of multi-fractured horizontal well with constant FBHP or constant production rate can be calculated. It is the properties of reservoir and fluid decides the distance travelled by pressure wave, and it is proportional to the time of production. Though many researchers have proposed the method of calculating the rate of pressure wave traveling in reservoir, none of them employ the definition to outer reservoir. In this section, two equations for DOI traveled within outer reservoir have been proposed for constant FBHP and constant flow rate conditions.

Geometry of the reservoir is shown is Fig. 3.1. The well is located at the middle of the hydraulic fracture, and the DOI first traveled within the fracture; when the DOI reaches the tip of fracture, DOI start to propagate from fracture to the mid-line of two

fractures. As soon as the DOI arrived the mid-line, from the contact between inner reservoir and outer reservoir it starts to propagate away from inner reservoir.

For the transient linear flow system, we employ the method called maximum rate of pressure response. A unit impulse of pressure is an impulse during a very short time. Both production of fluid or injection of fluid can initiate the impulse. If we set an observation point in the reservoir away from the production well, the objective is to determine the time of the maximum rate of pressure response arriving at the point, then the pressure wave propagating speed. In aspect of mathematics, the principle of superposition time can be employed to model the unit impulse. The expression of DOI can be determined by initiating a small impulse and observing t_{max}, the maximum pressure response happens at the observation point.

Since Eq. 3.64 is complex, it cannot be directly translated into an analytic solution, we employ numerical inversion (Stehfest et al. 1970) to transfer Eq. 3.49 and Eq. 3.64 from Laplace-transform space,

$$f(t)=\frac{\ln 2}{t}\sum_{i=1}^{N}V_i f(\frac{\ln 2}{t}\mathrm{i}) \quad \text{.....(3.66)}$$

$$V_i=(-1)^{\left(\frac{N}{2}-1\right)}\sum_{k=\left\lfloor\frac{i+1}{2}\right\rfloor}^{\min\left(i,\frac{N}{2}\right)}\frac{k^{\frac{N}{2}+1}(2k)!}{\left(\frac{N}{2}-k\right)!k!(k-1)!(i-k)!(2k-i)!} \quad \text{.....(3.67)}$$

Applying the numerical inversion, we can obtain the value of dimensionless pressure at each specific position at any time. In order to determine the DOI within the outer reservoir, we employ the theory of maximum rate of pressure response, which is the second derivative of dimensionless pressure with respect to dimensionless time, when

time equals zero， $d/dt_D\left(dp_D/dt_D\right)=0$. At first, we plot the relationship between dimensionless pressure and dimensionless time at each specific position within the outer reservoirs. By determining the time at which it satisfies the maximum rate of pressure response for each specific position, we can earn the time that DOI arrives at that position. Multiply DOI with the fracture spacing and reservoir thickness, coupled with the DDV of inner reservoir the advancement of the DDV within outer reservoir shows a linear relation with $\sqrt{t-t_e}$ (Fig. 3.3 and Fig. 3.4), where t_e is the time that DOI arrived the mid-lane of two adjacent fracture clusters.

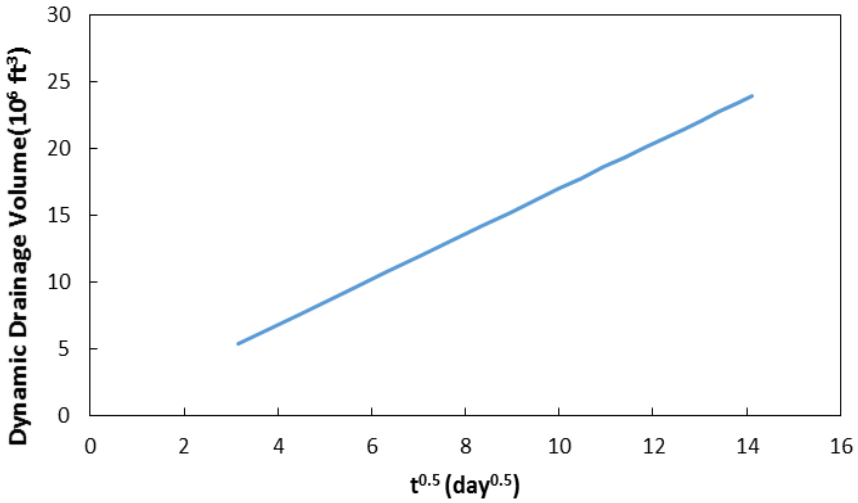

Figure 3.3 Change of DDV with respect to square root of time concluded out from analytical solution within SRV for constant-FBHP boundary condition

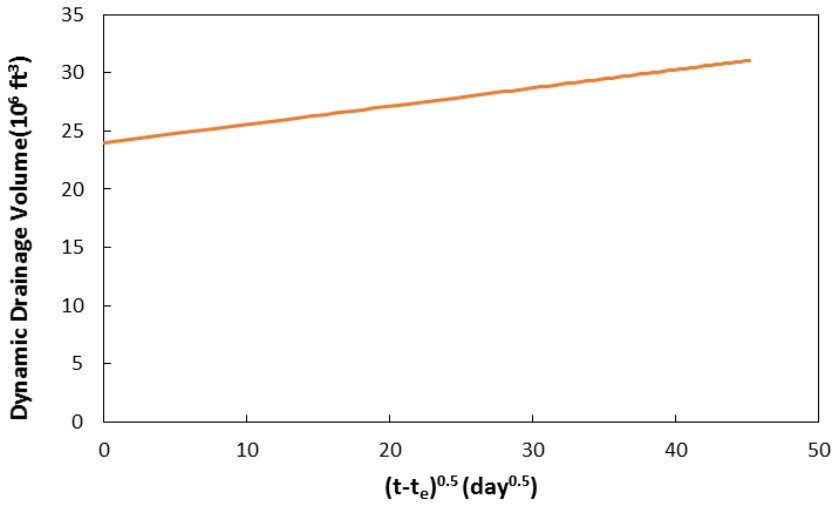

Figure 3.4 Change of DDV with respect to square root of time concluded out from analytical solution the within outer reservoir for constant-rate boundary condition

3.3 Analytical DDV Equation by Multivariate Regression

Different from the classical equation of DOI (DDV referred as volume) within SRV, the analytical solution for transient flow of multi-stage fractured horizontal well (MFHW) in the composite linear flow system is sophisticated. However, we can obtain the curve of DDV with respect to time by calculating the discrete points with the analytical solutions, as described above. It is still necessary to derive a practical analytical expression of DDV for the field applications. In this work, we apply the multi-variate regression to conclude the analytical solution of DDV for multi-stage fractured horizontal well.

As shown in Fig. 3.3, there is a linear relation between the DDV and square root of time, therefore, we just need to find the expression of the slope between DDV and square-root of time, coupled with the effects of various parameters, i.e., diffusivities of both the inner stimulated reservoirs and the outer matrix reservoirs, length of primary fracture, and fracture spacing. First, we assume the slope follows a representation of

$$Slope = C \cdot \eta_I^a \cdot \eta_O^b \cdot x_F^c \cdot y_e^d \quad \text{(3.68)}$$

where C is a constant, and, a, b, c, d are the fitting parameters indicating the contribution of different factors, i.e., η_I , η_O , x_F , y_e . Given the discrete points calculated by the above methods in Fig. 3.3, we find the optimal values of C, a, b, c, d to best approximate the data by applying the multivariate regression.

We take the natural logarithm on both sides of Eq. 3.68:

$$\ln(Slope) = \ln(C) \cdot 1 + a \cdot \ln(\eta_I) + b \cdot \ln(\eta_O) + c \cdot \ln(x_F) + d \cdot \ln(y_e) \quad \text{(3.69)}$$

Then, we construct a feature matrix X that has a size n by 5, where n is the number of data available to us, 5 is the number of features. We also assume Y is a column vector that contains the natural logarithm of slope in our data.

$$\mathrm{X} = \begin{bmatrix} 1 & \cdots & \ln(y_{e1}) \\ \vdots & \ddots & \vdots \\ 1 & \cdots & \ln(y_{en}) \end{bmatrix} \quad \text{(3.70)}$$

$$\mathrm{Y} = \begin{bmatrix} \ln(Slope_1) \\ \vdots \\ \ln(Slope_n) \end{bmatrix} \quad \text{(3.71)}$$

Then the final solution is given by:

$$\begin{bmatrix} \ln(C) \\ \eta_I \\ \eta_O \\ x_F \\ y_e \end{bmatrix} = (X^T X)^{-1} XY \quad \text{(3.72)}$$

In this work, to obtain enough accuracy in the solution, and after calculating 4000 cases of different combinations of parameters with analytical solutions, we implemented the multivariate regression method to find the best regression line.

For constant-pressure boundary condition, the empirical equation is:

$$Slope = 0.741712 \cdot \eta_I^{0.037256} \cdot \eta_O^{0.464276} \cdot x_F^{0.072896} \cdot y_e^{0.926067} \quad \text{.....(3.73)}$$

The comparison between the regressed expression of slope (Eq. 3.73) and the slope calculated by analytical solutions for all the 2000 cases is shown in Fig. 3.5, which indicates the precise accuracy of the empirical equation (Eq.3.73).

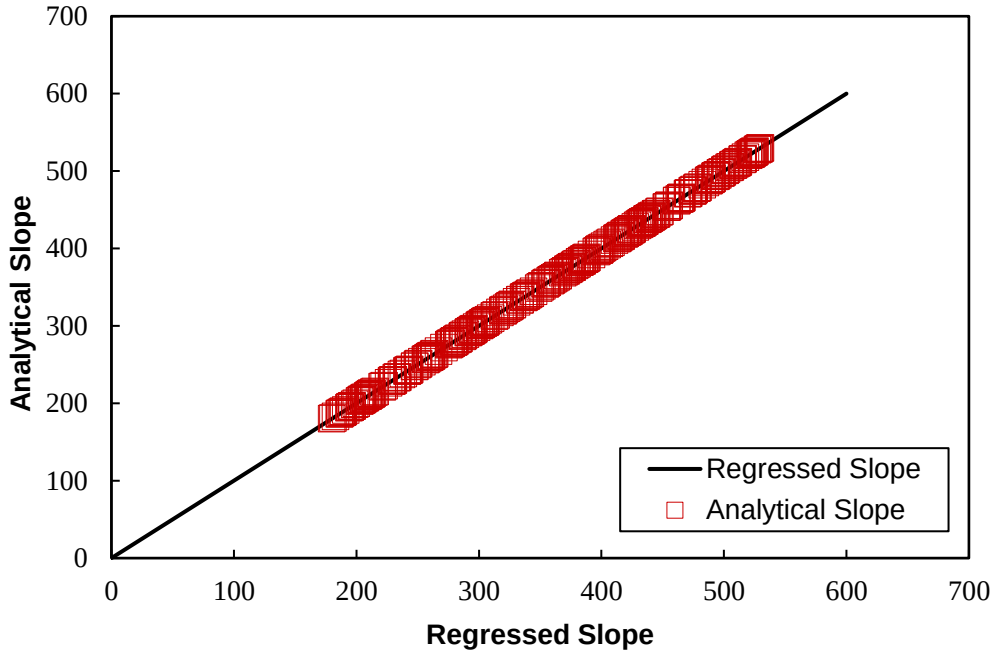

Figure 3.5 Comparison of regressed slope calculated by Eq. 3.37 and analytical slope calculated via analytical solution derived in this paper.

The empirical expression of Dynamic-Drainage-Volume (DDV) is shown as follows,

$$DDV = \begin{cases} 0.113 \times 4 x_f h \sqrt{(k/\phi\mu c_t)t}, & t \le t_e \\ 0.113 \times 4 x_f h \sqrt{(k/\phi\mu c_t)t_e} + 0.741712 \eta_I^{0.037256} \eta_O^{0.464276} x_F^{0.072896} y_e^{0.926067} (\sqrt{t - t_e})h, & t > t_e \end{cases}$$

.....(3.74)

Similarly, for the constant flow rate boundary condition, the regressed analytical equation can be obtained as:

$$Slope = 0.798359 \cdot \eta_I^{0.004378} \cdot \eta_O^{0.496359} \cdot x_F^{0.007957} \cdot y_e^{0.992005} \quad \text{.....(3.75)}$$

The comparison between the regressed expression of slope (Eq. 3.75) and the calculated value for all the 2000 cases is shown in Fig. 3.6. The excellent match also indicates the accuracy of Eq. 3.75.

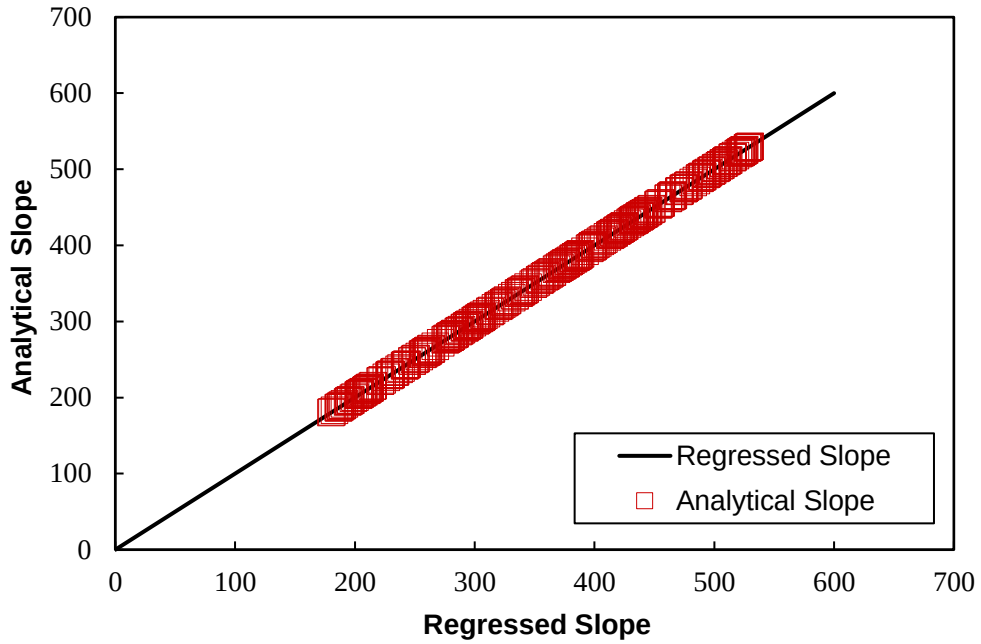

Figure 3.6 Comparison of slope calculated by Eq. 3.75 and true slope calculated via analytical solution derived in this paper.

Therefore, the empirical expression of Dynamic-Drainage-Volume (DDV) is shown as follows,

$$DDV = \begin{cases} 0.194 \times 4x_f h\sqrt{(k/\phi\mu c_t)t}, & t \le t_e \\ 0.194 \times 4x_f h\sqrt{(k/\phi\mu c_t)t_e} + 0.798359\eta_I^{0.004378}\eta_O^{0.496359}x_F^{0.007957}y_e^{0.992005}(\sqrt{t-t_e})h, & t > t_e \end{cases}$$

……...(3.76)

3.4 Model Verification

In this section, the new analytical and empirical expressions of DDV is verified against a synthetic fine-grid CMG model for the system addressed above – a multi-fractured horizontal well in a shale formation. In the process of conducting this

verification, difficulties were encountered in measuring the DDV of CMG model. The description of how to calculate the DDV in CMG has shown in this section.

Since there is only one phase fluid flow model, the black oil model is selected to build in CMG. As the assumption before, only a single fracture and its surrounding rectangular area is modeled, which is the same strategy described in Fig. 3.2. All the input parameters used for those two synthetic cases are listed in Table. 3.1. For this study, we assumed that the fracture has infinite conductivity and there are no skin effects. In addition, the diffusivity within SRV is much bigger than that of unstimulated (outer) reservoir volume, which is a common used assumption for fractured shale reservoirs. In order to account for the DDV, the CMG model is built in a fine grid type, size of 1ft*3ft. The summation of all the area of the grid with pressure decreasing more than 1 percent of initial pressure is the DDV we get from CMG model. Then we implement the regressed analytical equation proposed before to calculate the DDV for the two synthetic case. Fig. 3.6 and Fig. 3.7 show the comparison between results of regressed analytical solution and results of reservoir simulation.

Table 3.1 The values of input parameters for the synthetic fine-grid numerical simulation.

	Case1	Case2
permeability of inner fractured reservoirs, md	0.002	0.001
permeability of outer shale matrix, md	0.00004	0.00004
Reservoir porosity, decimal	0.06	0.075
Total compressibility, psi-1	1.6×10^{-5}	1.4×10^{-5}
Fracture length, ft	220	240
Fracture spacing, ft	60	80
Fluid viscosity, cp	0.4	0.4
Formation Thickness, ft	10	10
Initial reservoir pressure, psia	4405	4405
Inner-boundary condition, psia	400	
Inner-boundary condition, STB/day		10

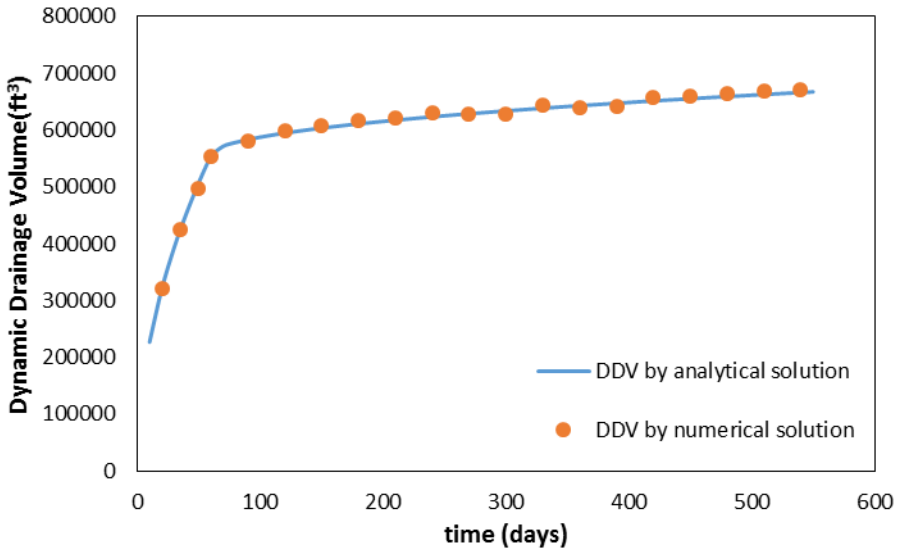

Figure 3.7 (Case1) Verification of empirical equation using CMG for constant flow rate constraint

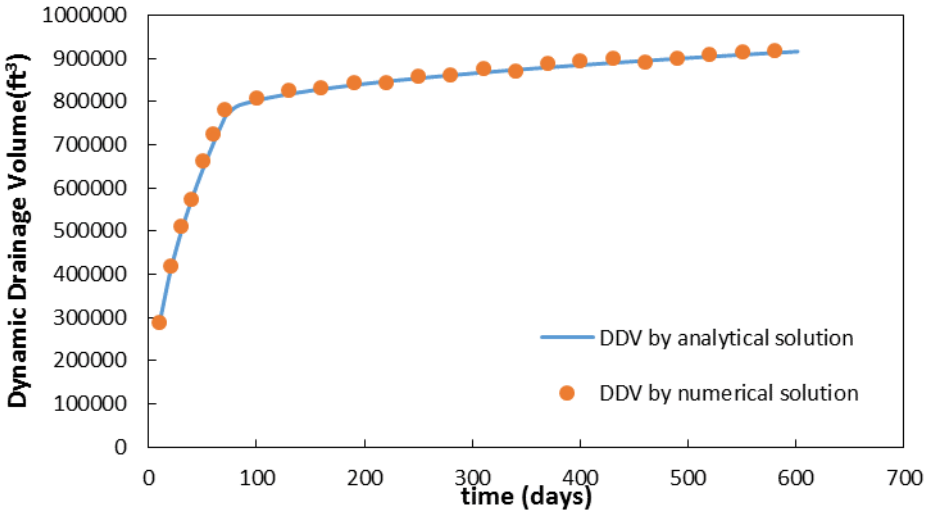

Figure 3.8 (Case2) Verification of empirical equation using CMG for constant flowing pressure constraint

3.5 Fracture Spacing Optimization

As indicated by the above regressed empirical equation, it is not difficult to separately study impact of various parameters on DDV. In this section, we make the sensitivity analysis of fracture spacing on DDV.

For the horizontal wells with same length, when we decrease the fracture spacing, correspondingly, the number of fractures will increase and the permeability of SRV will also increase because of the fracture interference (Zhao et al. 2014). To investigate the effects of fracture spacing on the enhanced conductivity within SRV, we use different conductivity (dispersion) for SRV for cases with various fracture spacing, as shown in Fig. 3.8. The relation between conductivity of SRV and fracture spacing has not been well understood yet (Zhao et al. 2015b); thus, the linear relationship is assumed here. Fig. 3.9 indicates the effects of different fracture spacing on the propagation of DDV within the compound linear flow system, and Fig. 3.10 amplifies the DDV of Fig. 3.9 within outer reservoir. The distance between fracture clusters can remarkably alter the speed of DDV advancement; however, this effect gradually disappears while the fracture spacing

becomes smaller. Despite the positive contribution of larger DDV by decreasing fracture spacing, it is not economically viable to create so many fracture clusters in a given length. The pattern indicated by Fig. 3.9 and Fig. 3.10 provides insight to optimize the fracture spacing by considering both the maximum DDV and the most economic efficiency.

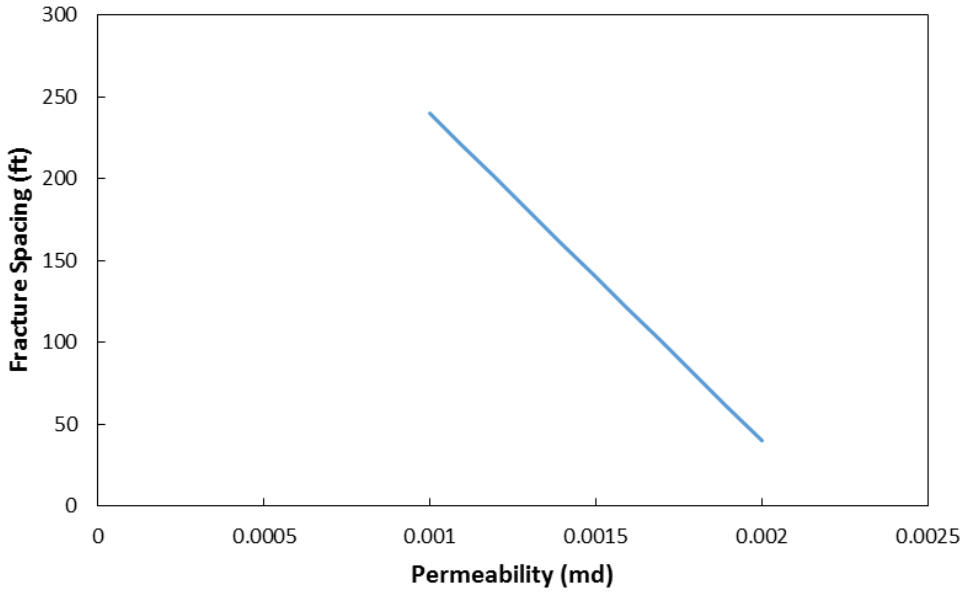

Figure 3.9 The synthetic relation between fracture spacing and permeability of SRV by considering fracture interference

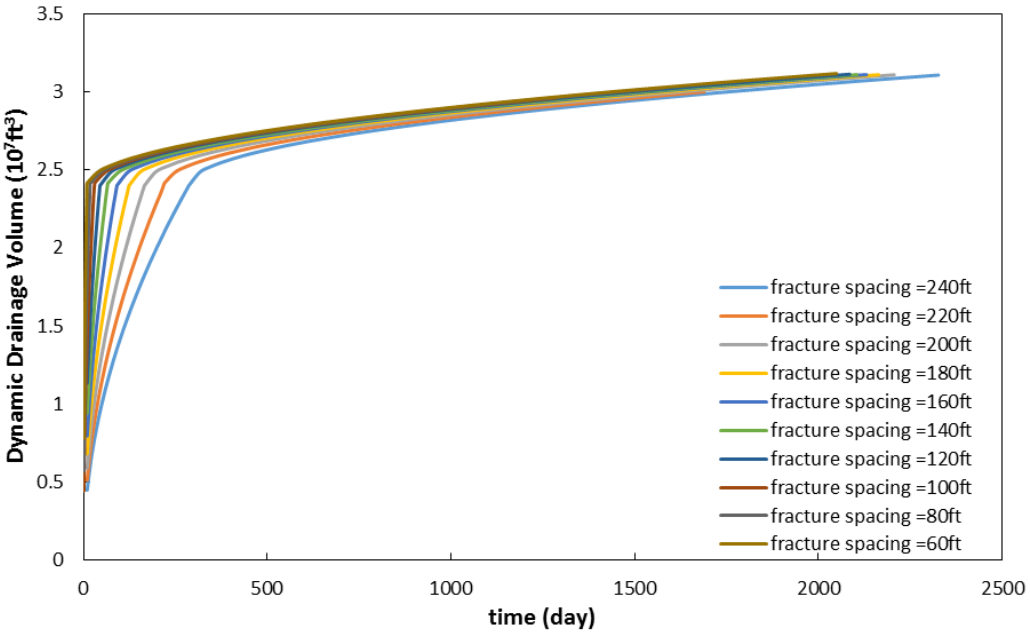

Figure 3.10 Influence of fracture spacing on the DDV of multistage horizontal well

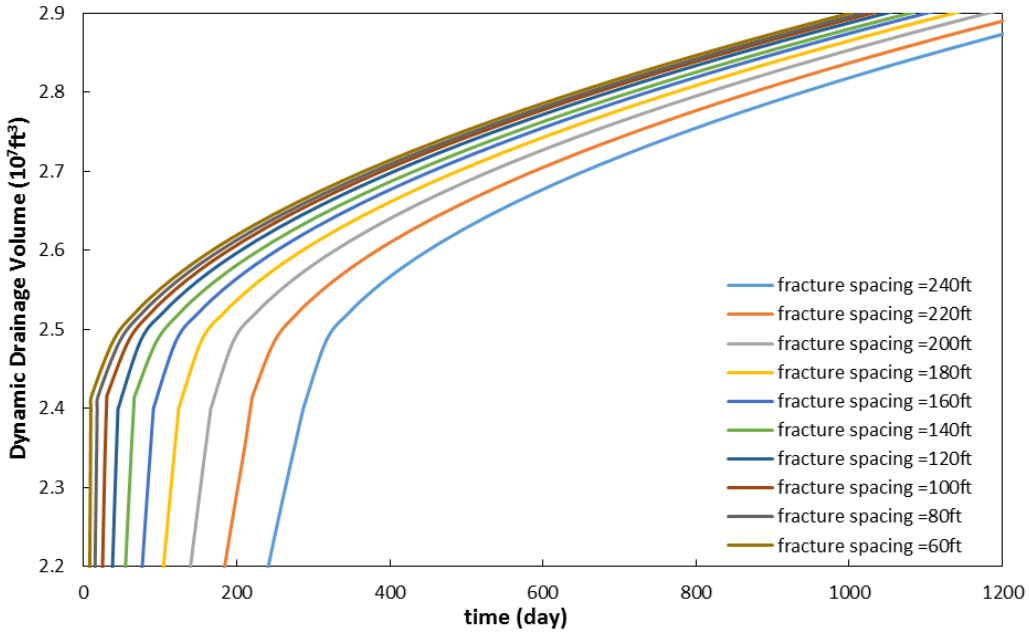

Figure 3.11 Amplification of Fig.9, influence of fracture spacing on the DDV of multistage horizontal well within outer reservoir

Chapter 4: Integrated Production Analysis

4.1 Macroscopic Compressible Tank Model

In ultra-low unconventional reservoir, transient-linear flow regime can last for several years, which contributes the majority of hydrocarbon production. During transient-linear flow, as the pressure disturbance created at the production well propagates throughout the reservoir, it will shape an expanding drainage volume (productive region). The boundaries of drainage volume are pushed back and the size of productive region grows as production continues. We treat the expanding drainage volume as a moving boundary problem. Therefore, the conventional material balance model is not able to be applied to calculate the average pressure and average saturation. In our mathematical model, the weak form (integral) of mass balance equation is specifically written for the expanding productive region. Fluid and rock compressibility, fracture properties, matrix permeability, and production rates are the factors controlling the speed at which the boundaries are advancing.

The mathematical description is derived in the most general form applicable to black oil, volatile oil and gas condensate reservoirs; however, the example will be for a black oil type of reservoir with neither adsorption nor volatile oil. In this study, our assumptions are as follows:

(1) The shale reservoir is isothermal, and there are three fluid components: stock-tank oil, surface gas and stock-tank water.

(2) The water component does not partition into the oleic phase, and the oil component does not partition into the aqueous phase.

(3) The adsorption phenomenon (for shale gas) can be explained through Langmuir isotherm.

(4) Stress-dependent porosity and permeability reservoirs contains slightly compressible fluid (pressure-dependent formation volume factor and fluid viscosity).

Different from the constant drainage volume during boundary-dominated flow, the dynamic drainage volume is always changing during long-term transient linear flow regime. Fig. 4.1 shows the difference among Stimulated-reservoir volume (SRV), Maximum-Drainage Volume (MDV) and well-control reserve. In general, the well spacing of MFHW is relative large during the primary depletion process by considering the economic costs. However, due to the effects of finite value of SRV and ultra-low permeability of unstimulated reservoir, the maximum drainage volume when the average reservoir pressure reaches the abandonment condition is much less than the well-control reserves determined by the well spacing. In other word, it takes extra-long time for MFHW flow in shale reservoirs to reach the physical flow boundary determined by well spacing. It is of great probability that MFHW is always in the transient-flow region for its well life until the abandonment condition. Therefore, it is desirable to accurately evaluate the changes of DDV with production time and predict the maximum drainage volume for the shale operators to make well optimization.

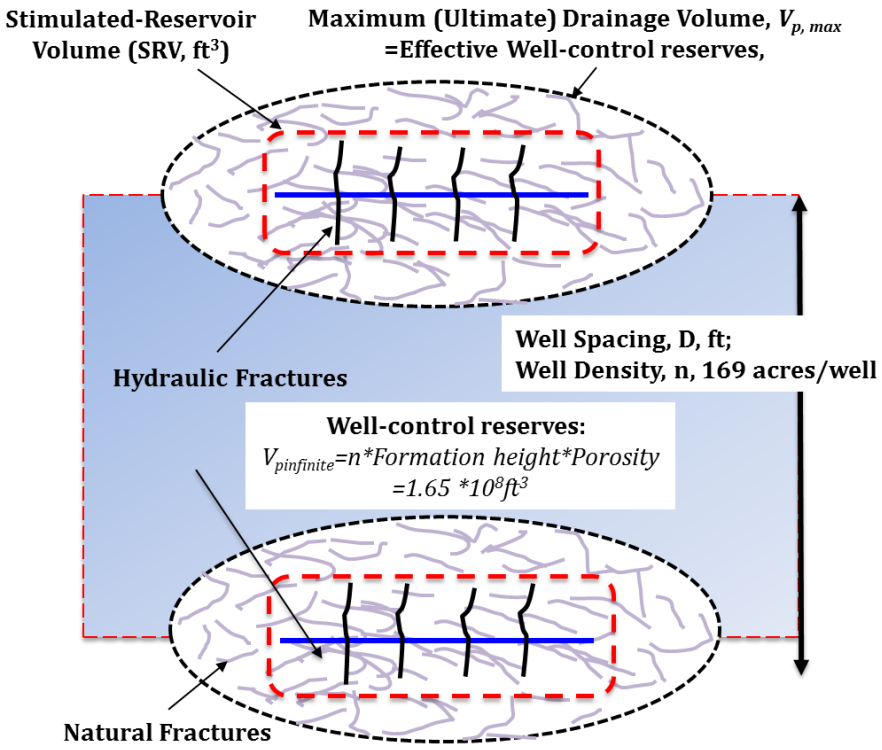

Figure 4.1 Multi-stage fractured horizontal wells with Stimulated-reservoir volume (SRV), and its maximum drainage volume ($V_{p,max}$) at abandon pressure, well-control reserves ($V_{P\infty}$) determined by well spacing

Transient flow is treated in succession of state method as Shahamat et al.(2014), but the problem of multiphase flow and variable operating condition is dealt with to enable the modeling of low-permeability liquid rich reservoirs(Clarkson et al. 2016). So the concept of dynamic drainage volume (DDV) can be implied here instead of 'succession of pseudo-steady states'. The DDV concept is illustrated in Fig. 4.2. For time step n, the DDV propagates to volume Vn. The material balance equation is used to solve for average pressure, average saturation of each phase. At time step n+1, the DDV has been propagated to volume Vn+1, and the calculation are repeated based on the results of last time step.

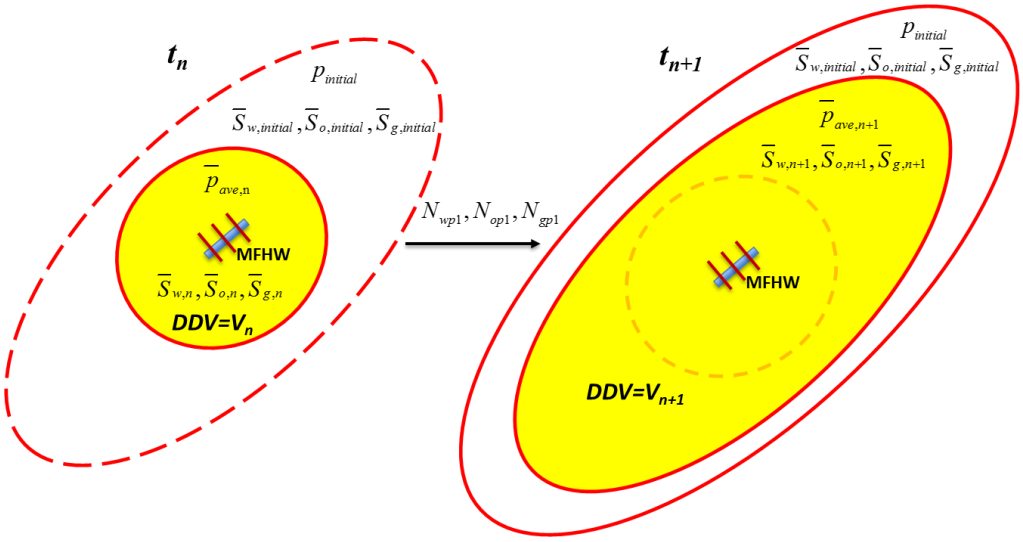

Figure 4.2 Schematic diagram of drainage volume expansion related to multistage fractured horizontal well (MFHW) in shale reservoirs during long-term transient flow regime

The water phase material balance is written as:

$$V_{(n)}\phi_i\left[1+c_f\left(p_{(n)}-p_i\right)\right]\left(\frac{\overline{S_{w(n)}}}{\overline{B_{w(n)}}}\right)+(V_{(n+1)}-V_{(n)})\phi_i\left(\frac{S_{wi}}{B_{wi}}\right)-V_{(n+1)}\phi_i\left[1+c_f\left(p_{(n+1)}-p_i\right)\right]\left(\frac{\overline{S_{w(n+1)}}}{\overline{B_{w(n+1)}}}\right)$$

$$=N_{wp(n+1)}-N_{wp(n)} \quad \text{.....(4.1)}$$

In this equation, $V_{(n)}\phi_i\left[1+c_f\left(p_{(n)}-p_i\right)\right]\left(\frac{\overline{S_{w(n)}}}{\overline{B_{w(n)}}}\right)$ is the water content of last time step, and $(V_{(n+1)}-V_{(n)})\phi_i\left(\frac{S_{wi}}{B_{wi}}\right)$ is the volume of water added to the reservoir tank because of advancing of DDV; $V_{(n+1)}\phi_i\left[1+c_f\left(p_{(n+1)}-p_i\right)\right]\left(\frac{\overline{S_{w(n+1)}}}{\overline{B_{w(n+1)}}}\right)$ is the volume of water in the DDV for current time step. The right-hand side of equation represents the production of water during the current time step.

The oil phase material balance equation is written as:

$$V_{(n)}\phi_i\left[1+c_f\left(p_{(n)}-p_i\right)\right]\left(\frac{\overline{S_{o(n)}}}{\overline{B_{o(n)}}}+\frac{\overline{S_{g(n)}}}{\overline{B_{g(n)}}}R_{v(n)}\right)+(V_{(n+1)}-V_{(n)})\phi_i\left(\frac{S_{oi}}{B_{oi}}+\frac{S_{gi}}{B_{gi}}R_{vi}\right)$$
$$-V_{(n+1)}\phi_i\left[1+c_f\left(p_{(n+1)}-p_i\right)\right]\left(\frac{\overline{S_{o(n+1)}}}{\overline{B_{o(n+1)}}}+\frac{\overline{S_{g(n+1)}}}{\overline{B_{g(n+1)}}}R_{v(n+1)}\right)=N_{op(n+1)}-N_{op(n)} \quad \text{.....(4.2)}$$

The term $V_{(n)}\phi_i\left[1+c_f\left(p_{(n)}-p_i\right)\right]\left(\frac{\overline{S_{g(n)}}}{\overline{B_{g(n)}}}R_{v(n)}\right)$ represent the volume of oil condensate from gas for last time step; similarly, the term $V_{(n+1)}\phi_i\left[1+c_f\left(p_{(n+1)}-p_i\right)\right]\left(\frac{\overline{S_{g(n+1)}}}{\overline{B_{g(n+1)}}}R_{v(n+1)}\right)$ represent the volume of oil condensate from gas for current time step. If the object reservoir is not gas condensate reservoir, the term representing oil come from condensate gas need to be discarded.

The gas phase material balance equation is written as:

$$V_{(n)}\phi_i\left[1+c_f\left(p_{(n)}-p_i\right)\right]\left(\frac{\overline{S_{g(n)}}}{\overline{B_{g(n)}}}+\frac{\overline{S_{o(n)}}}{\overline{B_{o(n)}}}R_{s(n)}\right)+(V_{(n+1)}-V_{(n)})\phi_i\left(\frac{S_{gi}}{B_{gi}}+\frac{\overline{S_{oi}}}{\overline{B_{oi}}}R_{si}\right)$$
$$-V_{(n+1)}\phi_i\left[1+c_f\left(p_{(n+1)}-p_i\right)\right]\left(\frac{\overline{S_{g(n+1)}}}{\overline{B_{g(n+1)}}}+\frac{\overline{S_{o(n+1)}}}{\overline{B_{o(n+1)}}}R_{s(n+1)}\right)=N_{gp(n+1)}-N_{gp(n)} \quad \text{.....(4.3)}$$

The term $V_{(n)}\phi_i\left[1+c_f\left(p_{(n)}-p_i\right)\right]\left(\frac{\overline{S_{o(n)}}}{\overline{B_{o(n)}}}R_{s(n)}\right)$ represents the volume gas resolved from oil as pressure drop down. So the term equals 0 if the pressure above bubble point pressure. Sum up those above three material balance equation for water, oil and gas phase into together, and obtain the general material balance equation,

$$
\begin{aligned}
&V_{(n)}\phi_i\left[1+c_f\left(p_{(n)}-p_i\right)\right]\left(\frac{\overline{S_{w(n)}}}{\overline{B_{w(n)}}}+\frac{\overline{S_{o(n)}}}{\overline{B_{o(n)}}}++\frac{\overline{S_{g(n)}}}{\overline{B_{g(n)}}}+\frac{\overline{S_{g(n)}}}{\overline{B_{g(n)}}}R_{v(n)}+\frac{\overline{S_{o(n)}}}{\overline{B_{o(n)}}}R_{s(n)}\right)\\
&+(V_{(n+1)}-V_{(n)})\phi_i\left(\frac{S_{wi}}{B_{wi}}+\frac{S_{oi}}{B_{oi}}+\frac{S_{gi}}{B_{gi}}+\frac{S_{gi}}{B_{gi}}R_{vi}+\frac{\overline{S_{oi}}}{\overline{B_{oi}}}R_{si}\right) \qquad \text{……(4.4)}\\
&-V_{(n+1)}\phi_i\left[1+c_f\left(p_{(n+1)}-p_i\right)\right]\left(\frac{\overline{S_{w(n+1)}}}{\overline{B_{w(n+1)}}}+\frac{\overline{S_{o(n+1)}}}{\overline{B_{o(n+1)}}}+\frac{\overline{S_{g(n+1)}}}{\overline{B_{g(n+1)}}}+\frac{\overline{S_{g(n+1)}}}{\overline{B_{g(n+1)}}}R_{v(n+1)}+\frac{\overline{S_{o(n+1)}}}{\overline{B_{o(n+1)}}}R_{s(n+1)}\right)\\
&=(N_{wp(n+1)}+N_{gp(n+1)}+N_{op(n+1)})-\left(N_{wp(n)}+N_{op(n)}+N_{gp(n)}\right)
\end{aligned}
$$

where V_p is the drainage pore volume in ft^3; B_o and B_w are the oil and water formation volume factor corresponding to the average pressure of DDV in bbl/STB; B_g is the gas formation volume factor corresponding to the average pressure of DDV in bbl/SCF; t is the production time in days; R_s is the dissolved gas-oil ratio at average pressure in SCF/STB; S_w, S_o, and S_g are the average water, oil and gas saturation within DDV; N_{wp}, N_{wp} and N_{gp} are the cumulative oil, water and gas production amount; n is the time step, day.

In this equation, for the last time step variables, the saturation of each phase can be calculated in last time step; the formation volume factor can be calculated based on the pressure of last time step. The initial variables are known at the beginning. Combined with $S_w+S_O+S_g=1$, the pressure and saturation of current time step can be calculated. According to fractional recovery factor (B.C. Craft et al., 1991), the dynamic recovery factor can be obtained by,

$$
RF_{(n)}=\frac{N_{p(n)}}{N}=\left[\frac{B_{t(n)}-B_{ti}}{B_{t(n)}+\left(R_{p(n)}-R_{si}\right)B_{g(n)}}\right]\left[\frac{V_{p(n)}}{V_{p,\max}}\right]=\frac{c_{t(n)}\left(p_i-\overline{p_n}\right)B_{ti}}{B_{t(n)}}\frac{V_{p(n)}}{V_{p,\max}} \qquad \text{…….(4.5)}
$$

There are two forms of equation to calculate the recovery factor. Different from the conventional model of recovery factor, this paper introduces the term of sweep

efficiency, i.e., the ratio of dynamic drainage volume to the maximum drainage volume at the condition of abandon pressure. In addition, after we get the maximum dynamic drainage volume at abandon reservoir pressure, it is feasible to apply Eq. 4.5 to determine the maximum (ultimate) recovery factor. Moreover, the changes of phase saturation need to be derived by the ratio of oil volume divided by the pore volume, as follows:

$$S_{o(n)} = \left(1 - RF_{(n)}\right)\left(1 - S_{wi}\right)\frac{B_{o(n)}}{B_{oi}};\ \ S_{g(n)} = 1 - S_{o(n)} - S_{wi};\ \ S_{w(n)} = S_{wi} \quad \text{.....(4.6)}$$

Followed by, the analytical model of DDV for early linear-flow within SRV and long-term transient flow for both SRV and unstimulated matrix, proposed in last section, can be substituted into the macroscopic model to evaluate the performance of MFHW.

Eq. 3.74, Eq. 3.76, and Eq. 4.1-4.6 form the system of macroscopic "tank model" by substituting all necessary equations into the key mass balance equation (Eq. 4.4). The inputs are: (1) oil, gas, and water production data; (2) total compressibility value; (4) fluid property data (B_o, B_g, B_w, as a function of pressure). As shown the flowchart of macroscopic model in Fig.4.3, we start the macroscopic code with an initial guess for average reservoir pressure at the first step, which should be barely less than the initial reservoir pressure. The process would be carried out via an iterative approach to calculate the drainage pore volume, V_p, and average pressure, $\bar{p}$ while the left side and right side of Eq.4.5 converge as close as possible at every certain production time reach the minimum value. The outputs of the macroscopic code include, dynamic drainage pore volume, V_p, average pressure, $\bar{p}$, phase saturation, S_w, S_o, and S_g, and recovery factor (RF) at different time.

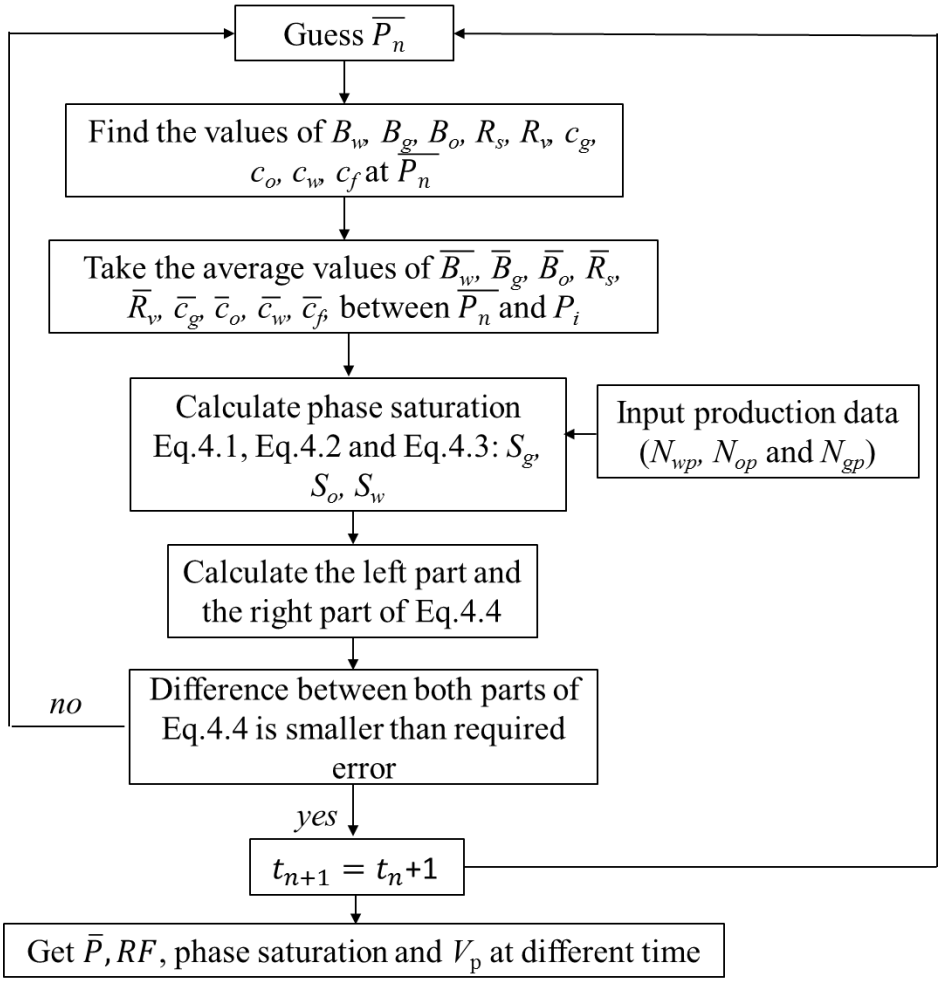

Figure 4.3 Flowchart of macroscopic to evaluate MFHW in shale reservoirs using production history and the concept of dynamic drainage volume

4.2 pseudo-variable and correction factor

In addition, for reservoirs with non-static reservoir properties and compressible fluids, the rock/fluid properties can be related to pressure as follows,

$$\begin{cases} B_o = B_{oi}\exp\left[-c_o\left(p_i-\overline{p}\right)\right] \\ \phi = \phi_i\exp\left[-c_f\left(p_i-\overline{p}\right)\right] \\ k = k_i\exp\left[-\gamma_k\left(p_i-\overline{p}\right)\right] \\ \mu_o = \mu_{oi}\exp\left[-c_\mu\left(p_i-\overline{p}\right)\right] \end{cases} \quad \text{.....(4.7)}$$

Where, B_{oi}, φ_i, k_i, μ_{oi} are the oil (formation volume factor, porosity and viscosity) and formation properties (permeability) at the condition of initial reservoir pressure; γ_k is the permeability modulus; c_o, is the oil compressibility; c_f, is the rock compressibility and c_μ is the fluid viscosibility (Schlumberger, 2010).

To eliminate the trouble to construct complex, variable-production-rate or variable-FBHP (superposition) solutions for the analysis of field production data. We need to introduce the use of material-balance time to make the production analysis variables (i.e., rate-normalized pressure (RNP), and production index etc.) as a weak function of production mode (variable rates or FBHP). In addition, to consider the varying effects of pressure-dependent reservoir/fluid properties (permeability, porosity, and fluid viscosity etc.), this paper defines pseudo-pressure, pseudo-time, and pseudo-material balance time as following.

$$m\left(\bar{p}\right)=\frac{\mu_{oi}B_{oi}}{k_i}\int_{p_i}^{\bar{p}}\frac{k_i\left(p\right)k_{ro}\left(S_o\right)}{\mu_o\left(p\right)B_o\left(p\right)}dp \quad \text{.....(4.8)}$$

$$t_a=\left(\frac{\phi\mu_o}{k}\right)_i\int_0^t\frac{k}{\phi\mu_o}d\tau \quad \text{.....(4.9)}$$

$$t_{ma}=\frac{\left(\frac{\phi\mu_o}{k}\right)_i}{q_{o,sc}}\int_0^t\frac{kq_{o,sc}}{\phi\mu_o}d\tau \quad \text{.....(4.10)}$$

As derived by Behmanesh et al. (2015), to simplify the use of pseudo-variables into production analysis workflow, it is desirable to approximate the relation between pseudo-material balance time and material-balance time, and the relation between pseudo-pressure and pressure, as follows:

$$t_a = \left(\frac{\phi\mu_o}{k}\right)_i \int_0^t \frac{k}{\phi\mu_o} d\tau = \left[\exp\left[\left(\gamma_k - c_f - c_\mu\right)\left(\overline{p} - p_i\right)\right]\right] t = f_{cp} t \quad \text{.....(4.11)}$$

$$t_{ma} = \frac{\left(\frac{\phi\mu_o}{k}\right)_i}{q_{o,sc}} \int_0^t \frac{k q_{o,sc}}{\phi\mu_o} d\tau = \left[\exp\left[\left(\gamma_k - c_f - c_\mu\right)\left(\overline{p} - p_i\right)\right]\right] t_m = f_{cp} t_m \quad \text{.....(4.12)}$$

$$f_{cp} = \left[\exp\left[\left(\gamma_k - c_f - c_\mu\right)\left(\overline{p} - p_i\right)\right]\right] \quad \text{.....(4.13)}$$

Where, the effects of non-static reservoir properties and compressible fluid properties have been included by correction factor, f_{cp}. All of them are functions of average reservoir pressure, which has been obtained by the above macroscopic code (Fig.4.3).

After the dynamic drainage volume and associated average reservoir pressure are obtained from the above macroscopic model, the transient-production index can be derived to demonstrate the decline characteristic for the long-term transient linear flow in unconventional reservoirs. Yuan et al. (2015) provides an empirical liquid production index and determine the values of constants for multiple flow regimes: a and n, during transient-linear (a= 0.8; n=2.5) and pseudo pseudo-steady state flow (a=0.8; n=1). In this paper, to couple the effects of pressure-dependent reservoir/fluid properties, following Araya and Ozkan (2002) and Medeiros et al. (2010), we define oil production index for oil-gas-water multiphase inflow performance relationship (IPR).

$$q_{o,sc} B_o = q_{b,sc} B_{ob} + \frac{J_l P_b}{na\left(1-a\right)^{n-1}} \left(1 - a\frac{P_{wf}}{P_b}\right)^n \quad \text{.....(4.13)}$$

$$\frac{B_o q_{o,sc}}{B_{o,\max} q_{o\max,sc}} = \left(1 - a\frac{P_{wf}}{P_b}\right)^n \quad \text{.....(4.14)}$$

$$q_{w,sc} B_w = J_l(t)\left(\overline{P} - P_{wf}\right) \quad \text{.....(4.15)}$$

Where,

$$q_b B_{ob} = J_l(t)\left(\overline{P} - P_b\right) \quad \text{.....(4.16)}$$

Hence, the liquid production index (PI) is

$$J_l(t) = \frac{q_{o,sc} B_o + q_{w,sc} B_w}{\left(1 - f_w\right)\left(\overline{P} - P_b + \frac{P_b}{na(1-a)^{n-1}}\left(1 - a\frac{P_{wf}}{P_b}\right)^n\right) + f_w\left(\overline{P} - P_{wf}\right)}, \quad \text{.....(4.17)}$$

Here, $q_{o\max,sc}$ is the maximum surface production rate at the IPR curve, STB; $B_{o,\max}$ is the oil formation factor at the condition of $q_{o\max,sc}$, bbl/STB; a and n are the empirical factors to be determined for different flow regimes; B_{ob} is the oil formation factor at the bubble-point pressure condition, bbl/STB; $J_l(t)$ is liquid production index, STB/(day·psia); $\overline{P}$ is the average pressure within the expanding drainage volume at time t.

As discussed before (Medeiros et al. 2010), the plot of transient-production index (Eq.4.17) with production time should be different for different flow regimes (i.e., the dominated transient-linear and pseudo pseudo-steady state flow regime in unconventional reservoirs). Therefore, we can estimate the fracture/reservoir properties from the above transient-production index curves.

4.3 Rate-Normalized Pseudo-Pressure Analysis (RNP)

Based on the derivation and modification of pseudo-variables and mathematical model, rate-normalized pressure analysis (RNP), which is applicable to variable production rates and FBHP conditions, can be conducted to interpret the flow regimes of fractured horizontal wells characterizing different flow patterns and fracture/reservoir parameters. Rate-normalized pressure is easily computed with given production data and is more straightforward to analyze than pressure-normalized rate (Song et. al 2011). Before the distance of investigation (DOI) arrive the mid-line of two adjacent fractures, the line of RNP derivative vs. time is in a ½ slope trend. For pseudo pseudosteady state, it shows a straight trend less than unit slope. The rate-normalized pressure and its derivative is calculated as:

$$RNP = \frac{p_i - p_{wf}(t)}{q(t)}$$

…… (4.18)

$$RNP' = \frac{dRNP}{d\ln t_e} \quad \text{.....(4.19)}$$

RNP and the derivative of RNP represent the production behavior that could be observed as a constant production rate.

Since the bottom hole pressure is decreasing during the production life of an oil/gas well, Palacio and Blasingame (1993) defined the material balance time as the ratio of Cumulative production (Q) to instantaneous production rate (q), in order to match the production data with Fetkovich type curve under a varying flowing pressure. The material balance time is defined as:

$$t_e = \frac{Q(t)}{q(t)} \quad \text{(4.20)}$$

This time function works very well for the scenarios that bottom hole pressure changing smooth. In order to couple the pressure-based property of fluid into the equation, we employ the rate-normalized pseudo-pressure and pseudo-material balance time, as follows:

$$m(RNP) = \frac{m(p_i) - m(p_{wf})}{q_{o,sc}(t)} \quad \text{(4.21)}$$

$$t_{ma} = f_{cp} \frac{N_p(t)}{q_{o,sc}(t)} \quad \text{(4.22)}$$

Using production date to log-log plot $m(RNP)$ against pseudo-material balance time (t_{ma}), and check the half-slope and almost unit-slope indicating the early transient-linear flow and later transient-linear flow regime. The accurate identification of multiple flow regimes can help us to integrate other specialty plots to evaluate the reservoir/fracture properties and well performance, such as transient-production index plot, semi-log radial derivative plot, linear plot and log-log dynamic-drainage-volume plot etc. Based on the end of linear flow regimes, and combined the known fracturing cluster spacing and equation of DDV, we can calculate the value of permeability within the stimulated-reservoir volume.

4.4 Square-root-of-time Plot

During transient-linear flow regimes, according to the analytical pressure solution from El-Banbi and Wattenbarger (1998), the pressure responses with modified pseudo-variables can be expresses as,

$$m\left(p_{wf}\right)=m\left(p_i\right)-\sqrt{f_{cp}}\,\frac{39.83q_{o,sc}}{h_f x_f\sqrt{\left(k\phi\mu_o c_t\right)_i}}\sqrt{t} \quad \text{.....(4.23)}$$

The effective fracture length can be obtained from:

$$x_f=\frac{39.83}{h_f m_L\sqrt{\left(k\phi\mu_o c_t\right)_i}} \quad \text{.....(4.24)}$$

In this equation, m_L is the slope of $\left[m\left(p_i\right)-m\left(p_{wf}\right)\right]/\left(q_{o,sc}f_{cp}\right)$ *vs* $\sqrt{t}$. To account for the changing reservoir and fluids properties, the introduction of $\sqrt{f_{cp}}$ is used to correct the estimated fracture length from conventional square-root-of-time plot ($\left[p_i-p_{wf}\right]/q_{o,sc}$ *vs* $\sqrt{t}$).

4.5 Iterative Approach to Evaluate Fracture Length

The accurate estimation of fracture length is important for analyzing the production data, since it is the key factor that affect the DDV propagation, then average pressure and average saturation.

Based on the dynamic drainage volume model and macroscopic “tank model”, the fracture length can be calculated with production data. As shown in Fig. 4.4, different from the method of conventional production data analysis, we need couple the effect of

pressure-dependent variables into the novel integrated production data analysis workflow.

When calculating the pseudopressure (Eq. 4.8), there is a complication that the relative permeability included is a saturation dependent variable. So the relationship between average pressure and average saturation is required to integrate the saturation dependent variables over pressure. Clarkson (2013) propose that the relative permeability is not a function of pressure. Some recent study indicates that the relationship between average saturation and average pressure remains unchanged during the complete transient flow period (Qanbari and Clarkson 2013; Behmanesh et al. 2015). Moreover, it is reasonable to assume that the relationship is independent of production history for practical propose. Qanbari (2013) and Behmanesh (2015) have already derived a relationship between saturation and pressure with production data and two-phase flow history. Clarkson (2016) proposed a new empirical relationship. In this paper, we proposed a new method calculating the relationship based on each specific case of different reservoirs. Employing the macroscopic code, the average saturation and average pressure of each production time could be calculated; then we can directly get the relationship between them.

The procedure (Fig. 4.4) of evaluating the fracture length is shown below:

1. According to the relationship calculated above, draw the plot $(p_i - p_{wf})/q_{osc}$ vs. Q/q to identify the flow regime. Find out the time when DOI reaches the midline of two adjacent hydraulic fractures, and calculate the permeability of stimulated reservoir volume (SRV) by Eq. 2.74 and Eq. 2.76.

2. Guess a fracture length and input it into macroscopic “tank model”, then calculate the relationship between average saturation and average pressure.
3. Draw the plot, RNP vs. square-root of material-balance-time (t_{ma}), and find out the slope m.
4. Supposing that the correction factor (f_{cp}) equals to 1 at beginning, the fracture length can be calculated via Eq. 4.24, which is an approximate value for the reason that correction factor is not real.
5. Input the new fracture length calculated last step into macroscopic tank model, and find out the average pressure and average saturation for each time interval.
6. Draw the plot $\frac{\triangle m / q_o(t)}{f(p)}$ vs. $\sqrt{t}$, and find out the new slope m of early time points (DDV does not reach outer reservoir).
7. Input m into step 4 to iterate until the error of fracture length within required discrepancy.

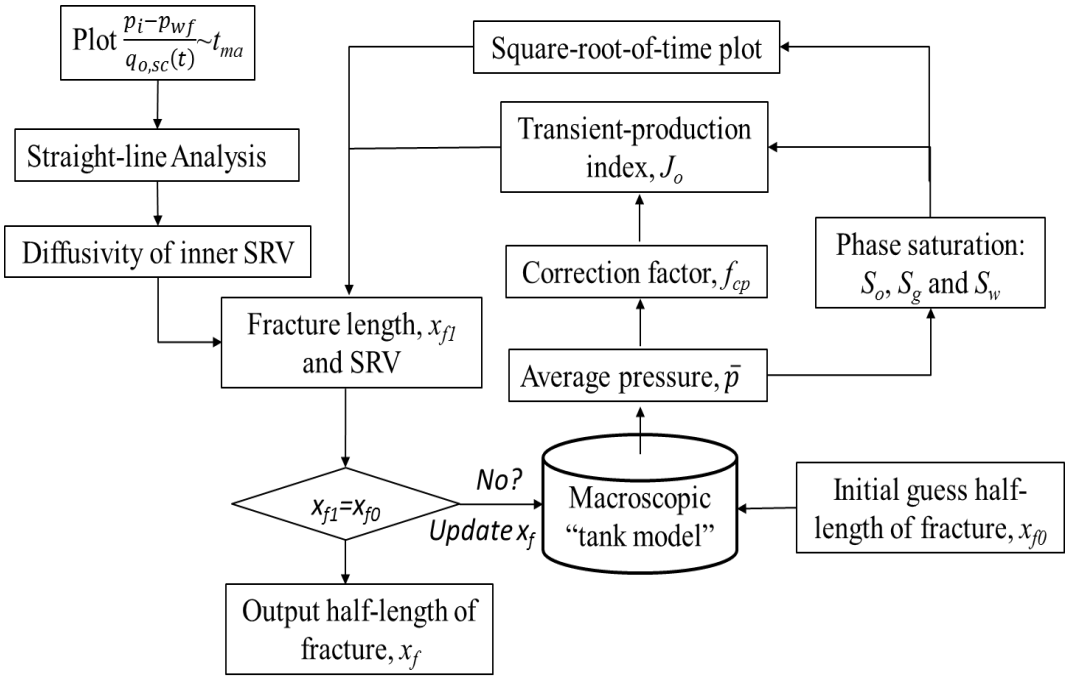

Figure 4.4 Determination of fracture length and diffusivity of inner SRV using iterative algorithm

4.6 Integrated Production Data Analysis Workflow Using DDV

As describe above, in order to perform integrated production data analysis of an unconventional reservoir, we have introduced the effects of stress-dependent reservoir properties and pressure-dependent fluid properties. The permeability of stimulated reservoir volume (SRV) and the fracture length have been estimated. The new macroscopic tank model is derived by using the concept of dynamic-drainage-volume (DDV) during the long-term transient flow of MFHW in shale reservoirs.

It is also necessary to quantify the contribution of fluid flow of the outer unstimulated matrix into the MFHW. We force the fluid flow only happens within inner reservoir, and apply macroscopic "tank model" to calculate the average pressure. Comparing the average pressure with and without outer reservoir, the contribution of outer reservoir can be quantified.

In addition, we apply the decline-curve-analysis to predict the future production rates, and combined with the abandonment condition (i.e., minimum production rate), we can also predict the ultimate recovery factor, the maximum drainage volume and associated average reservoir pressure at abandonment. The general procedure of integrated production data analysis is shown in Fig. 4.5.

One of the objectives in this production data analysis system is to estimate the long-term drained volume for a well in production. In this process an infinite drainage pore volume, the maximum amount of volume that could ever be affected, was estimated as is seen in Eq. 4.25. In case of the linear flow assumption in our above integrated production analysis, the modified Duong linear flow model (Eq. 4.25) (Duong 2010 and Joshi 2012) is used to make predication combined with the above production analysis workflow.

$$\frac{q}{Np} = at^{-m} \quad \text{(4.25)}$$

The parameters a and m can be determined using regression analysis by the plot between the left part of Eq.4.25 and the production time. Followed by, the initial production rate, q_1, can be determined by plotting the flow rates versus *t (a, m)* through Eq.26and Eq.27,

$$q = q_1 t(a,m) + q_\infty \quad \text{(4.26)}$$

$$t(a,m) = t^{-m} e^{\frac{a}{1-m}\left(t^{1-m}-1\right)} \quad \text{(4.27)}$$

The modified Duong's DCA method is to set the intercept of the regresses line as zero to offset the effects of short-term production history (6-12 months). It has been justified that

the setting of q_∞ as zero works better to make predication in most of field cases (Joshi, 2012)

After we get the empirical Duong's model using production history, then we can predict the future performance of MFHW. In this paper, we assume the minimum economic production rate as 10 STB/D for the well abandonment condition. We combine the predict production data with the above macroscopic code to evaluate the maximum drainage volume (MDV), associated average reservoir pressure within MDV, and the ultimate recovery factor for this MFHW.

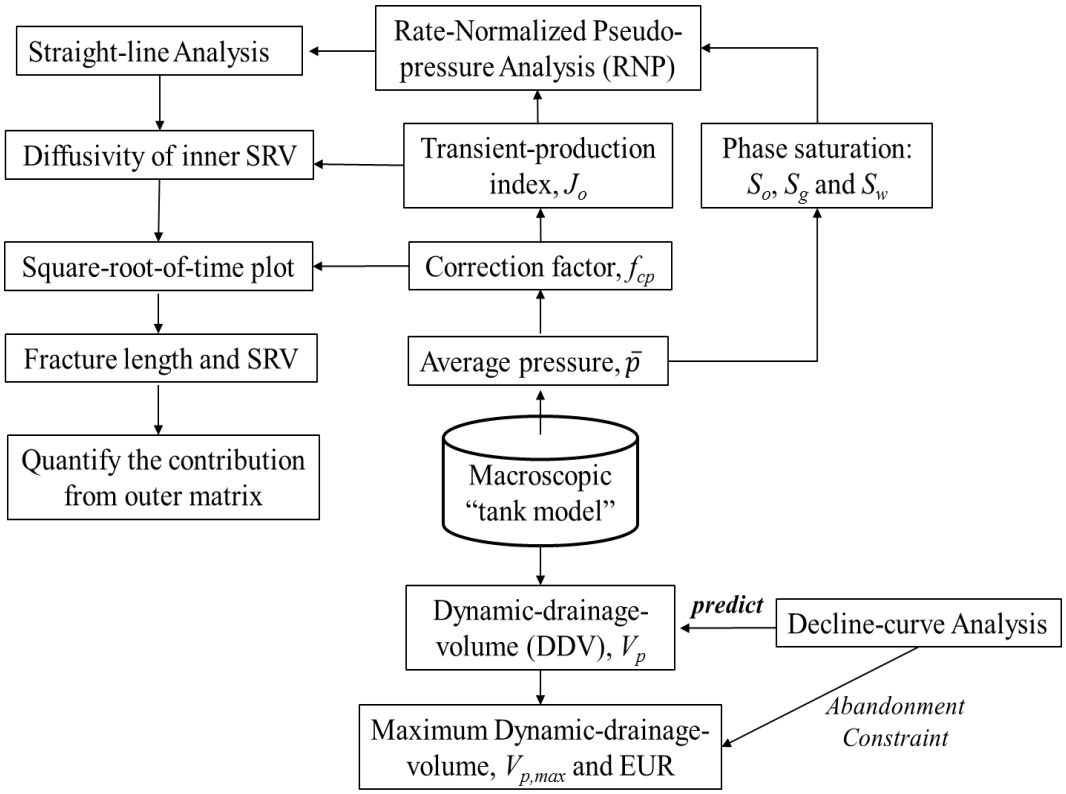

Figure 4.5 General procedure of integrated production data analysis

4.7 Model Validation with Synthetic Example

Firstly, to validate the new formula of DDV and new workflow of integrated production data analysis discussed as above, a synthetic example using fine-grid

numerical simulation is conducted. The basic parameters used in the synthetic model is summarized in Table.1. In this paper, we assume that the primary fracture has infinite conductivity. The early transient-linear flow within SRV is perpendicular to the primary fracture, and the late compound linear flow with moving boundary is perpendicular to the SRV. The contribution of fluid flow in the outer unstimulated matrix is not substantial but cannot be neglected.

Table 4.1 The values of input parameters for the synthetic fine-grid numerical simulation

Parameters	Synthetic Case
Permeability of inner SRV, md	0.002
Permeability of outer shale matrix, md	0.00004
Reservoir porosity, decimal	0.06
Total compressibility, psi-1	1.6×10^{-5}
Half-length of fracture, ft	220
Fracture spacing, ft	120
Fluid viscosity, cp	0.4
Formation Thickness, ft	10
Initial reservoir pressure, psia	4400
Constant FBHP condition, psia	200
Bubble-point pressure, psia	1000
Temperature, F	250
API_oil	45.4
Gas gravity	0.8
water density, lb/ft^3	59.3

As shown in Fig. 4.4, using the production data calculated by numerical simulation, we can obtain the propagation of DDV and associated average reservoir pressure. Fig. 4.6 and Fig. 4.7 shows the comparison of DDV and average reservoir pressure obtained by both the macroscopic model and numerical simulation. For calculating the average pressure of reservoir in synthetic CMG model, total DDV is calculated by counting the grid with pressure drop more than 1%, and average pressure is calculated by estimate the arithmetic average pressure of all the grid accounted as DDV.

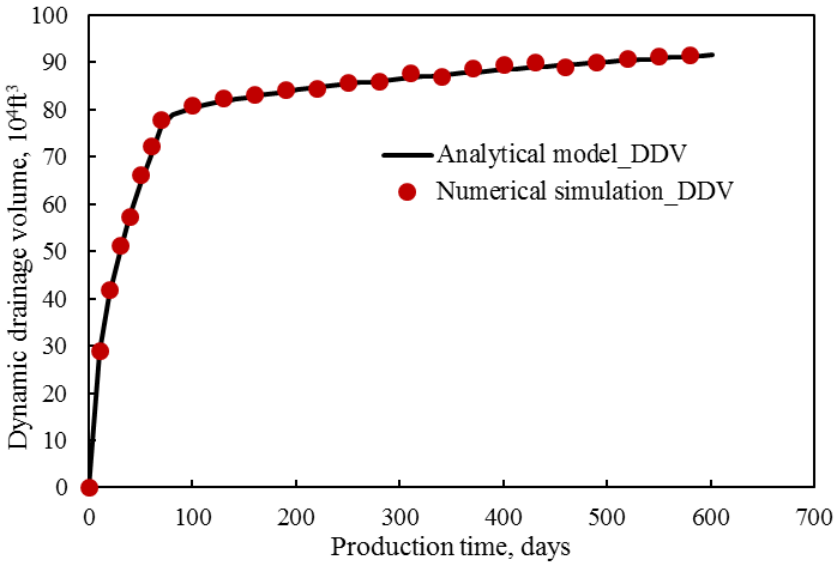

Figure 4.6 Comparison of DDV obtained from both analytical DDV model using production data and the direct evaluation of DDV from numerical simulation

In Fig. 4.7, for the case without the fluid flow contribution within the outer unstimulated matrix to the production of MFHW, the average reservoir pressure at the late production period of MFHW is less than the actual average reservoir pressure history obtained by numerical simulations. It indicates that the ignorance of fluid flow within the outer matrix for MFHW in shales can bring great error to the results of production data analysis. This synthetic example demonstrates the accuracy of our new proposed analytical DDV model. In addition, the calculated half-length of primary fracture using (no correction) (235 ft) and evaluated at average reservoir pressure within the DDV (218 ft) are compared with the input parameter to numerical simulation (220 ft). It is clear that the uncorrected fracture length by pressure-dependent correction factor is great than the expected fracture half-length.

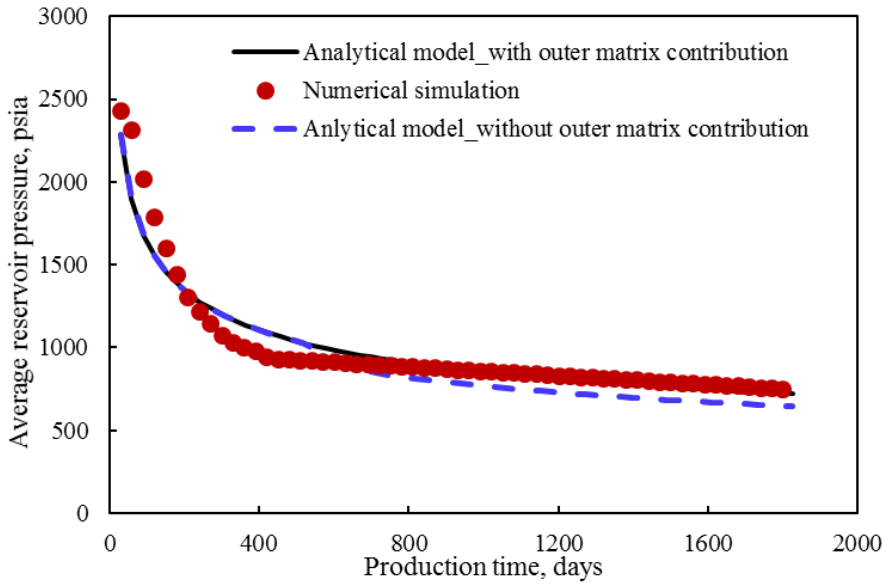

Figure 4.7 Comparison of average reservoir pressure within DDV obtained from both analytical DDV model by considering the fluid flow within the outer matrix or no fluid flow, and their comparison with the results obtained by numerical simulation

Chapter 5: Model Application and Field Case Study

In this chapter, the dynamic drainage volume (DDV) model and integrated production data analysis system proposed in chapter 3 and chapter 4 will be employed to calculate and analyze some real shale plays in United States. The permeability of stimulated reservoir volume and fracture half-length are evaluated; and the average pressure and average saturation are calculated with respect to different time. Prediction of ultimate DDV and ultimate estimated ultimate recovery (EUR) are conducted; then based on the information estimated above, fracture spacing and well spacing optimization are implemented.

This chapter presents the detailed analysis procedure for a single well and then show the results of analyzation of other 9 multi-fractured horizontal wells located in the same oil shale reservoir. The production time of these wells are different; some last for more than 1000 days and some last for as short as 400 days. Calculating all the production wells, this thesis compares the results and make some relative conclusion.

5.1 Evaluation of Production History

Herein the production history of a single MFHW is analyzed, and the detail of analyzing procedure is described. Table 5.1 represents some basic parameters of the reservoir and fluids in field units.

Table 5.1 The values of input parameters for a MFHW in Niobrara shale oil play in US

Parameters	Synthetic Case
Initial oil saturation/gas saturation	0.7/0.3
Permeability of outer shale matrix, md	0.00001
Reservoir porosity at initial reservoir pressure, decimal	0.075
Water compressibility, psi-1	3.4×10^{-6}
Formation compressibility, psi-1	1×10^{-5}
Half-length of fracture, ft	220
Fracture spacing, ft	54
Oil viscosity at the initial reservoir condition, cp	1.0
Formation Thickness, ft	500
Initial reservoir pressure, psia	7030
Coefficient of oil viscosity	1×10^{-5}
Coefficient of reservoir permeability	4×10^{-4}
Bubble-point pressure, psia	2500
Temperature, F	250
API of oil	45.4
Gas gravity	0.8377
Water density, lb/ft^3	59.3
Well length of MFHW, ft	5076
Number of fracture clusters	94

At first, draw the plot RNP ($(q_i - q_{wf})/q_{osc}$) vs. material balance time (Q/q) and RNP' vs material balance time (Fig. 5.1). It is straightforward to identify flow regime using straight-line analysis. There is an almost half-slope line reflecting linear flow, and followed by the late time compound-linear flow regime having slope equals to one. The

reason why it is not perfectly slope of ½ and slope of 1 is that outer reservoir fluid flow contributes to the total production during the linear flow status within inner reservoir. As the end time of linear flow (292 days) within SRV indicated by Fig. 5.1, we apply the DDV model in Eq. 5.1 (Behmanesh et al. 2015) to calculate the permeability of inner stimulated-reservoir volume (0.001mD).

$$y_{inv} = 0.194\sqrt{(k/\phi\mu c_t)t} \quad \text{.....(5.1)}$$

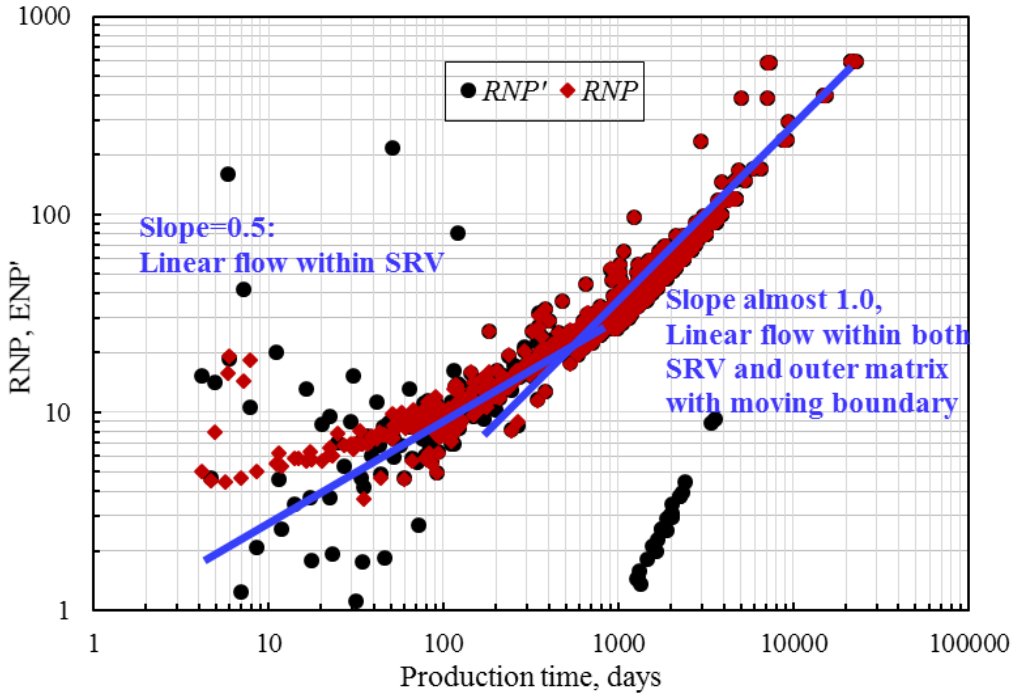

Figure 5.1 Rate-normalized pressure (RNP) analysis and rate-normalized pressure derivative (RNP') for MFHW in one of shale plays. Noted the x axis is material balance time.

Followed by, the fracture half-length is obtained by using the iterative algorithm as shown in Fig. 4.3 and Fig. 4.4. The estimated fracture half-length is 263 ft. The propagation of DDV, associated average reservoir pressure and phase saturation are obtained as a function of time, shown in Fig. 5.2 to Fig. 5.4. In order to quantify the contribution of outer reservoir fluid flow to well production, a hypothetical case that DDV is restricted to the volume of inner reservoir is conducted, i.e. there is no fluid flow from

outer matrix to inner reservoir (Fig. 5.2). If we neglect the contribution from the outer reservoir, the calculated average pressure is smaller and decrease more rapidly that that of the actual situation (Fig. 5.3). As a result, the free gas saturation below the bubble-point pressure increases more rapidly than that of actual case with the contribution from the outer matrix.

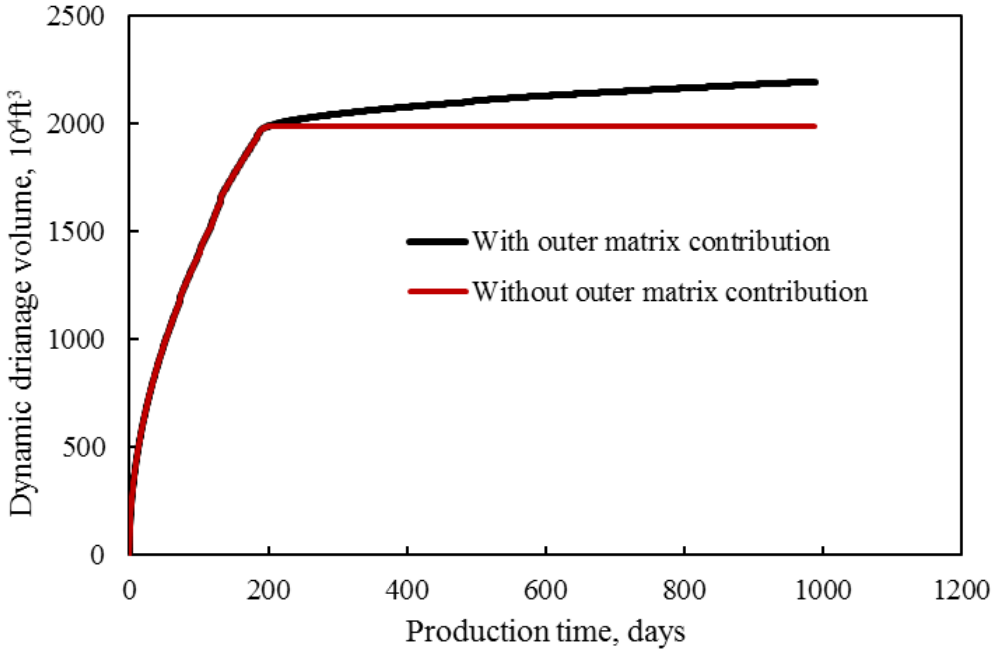

Figure 5.2 Results of DDV obtained from integrated production data analysis for two cases, Case 1: with the fluid flow contribution in the outer matrix and Case 2: without the fluid flow contribution in the outer matrix.

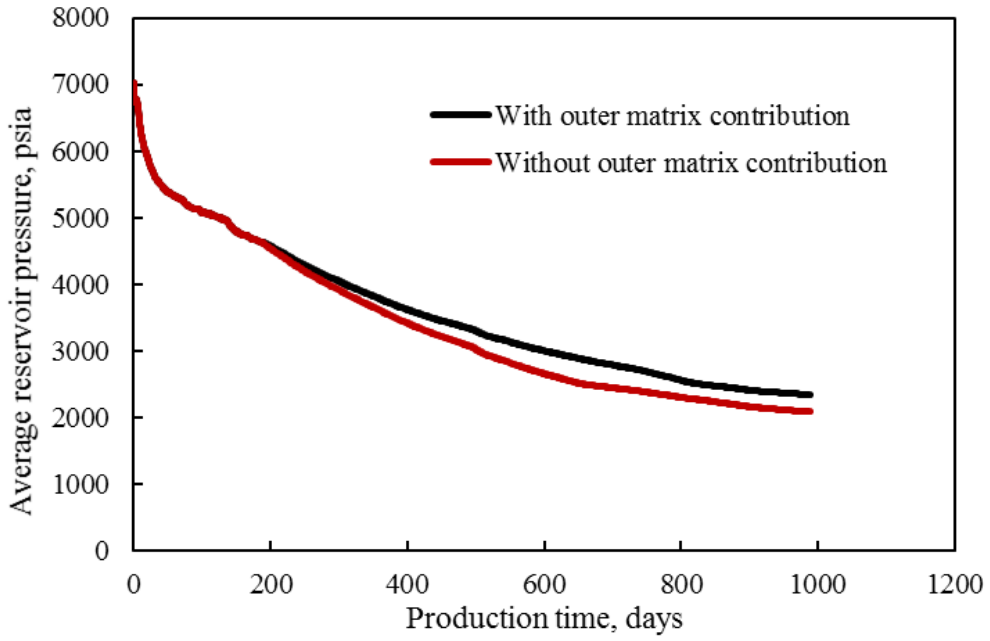

Figure 5.3 Graph of average reservoir pressure obtained from integrated production data analysis for two cases, Case 1: without the fluid flow contribution in the outer matrix and Case 2: with the fluid flow contribution in the outer matrix.

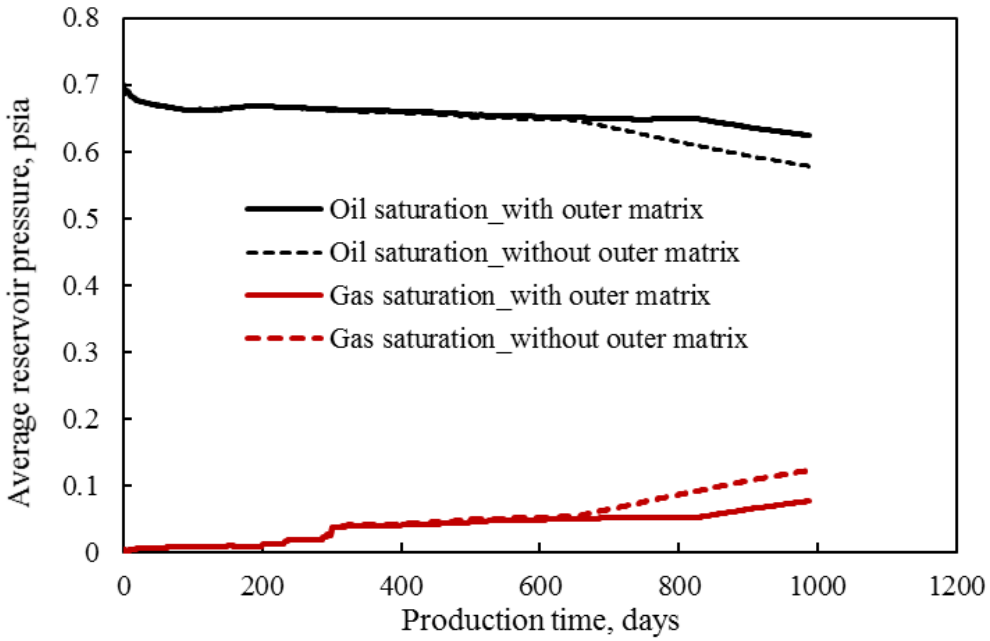

Figure 5.4 Graph of oil/gas phase saturation obtained from integrated production data analysis for two cases, Case 1: without the fluid flow contribution in the outer matrix and Case 2: with the fluid flow contribution in the outer matrix.

In addition, because the RNP analysis graph (Fig. 5.1) cannot demonstrate the effects of changing average reservoir pressure, as described by Eq.3.18. After we have obtained the change of average reservoir pressure, the transient-production index (Eq. 3.17) can be calculated as a function of time with the effects of average reservoir pressure, as shown in Fig. 5.5. In Fig. 5.5, there is also linear relationship between transient-production index and material-balance production time, but the slopes of linear relationship for the early linear-flow and the late compound-linear flow are different. The intersection point of those two lines indicates the end time of linear flow within SRV, which is 285 days (similar with the 292 days obtained by straight-line analysis in Fig. 5.1). This comparison confirms that the pressure-dependent correction factor does not affect the end time of linear flow within SRV, and it just bring difference to the magnitude of fracture half-length.

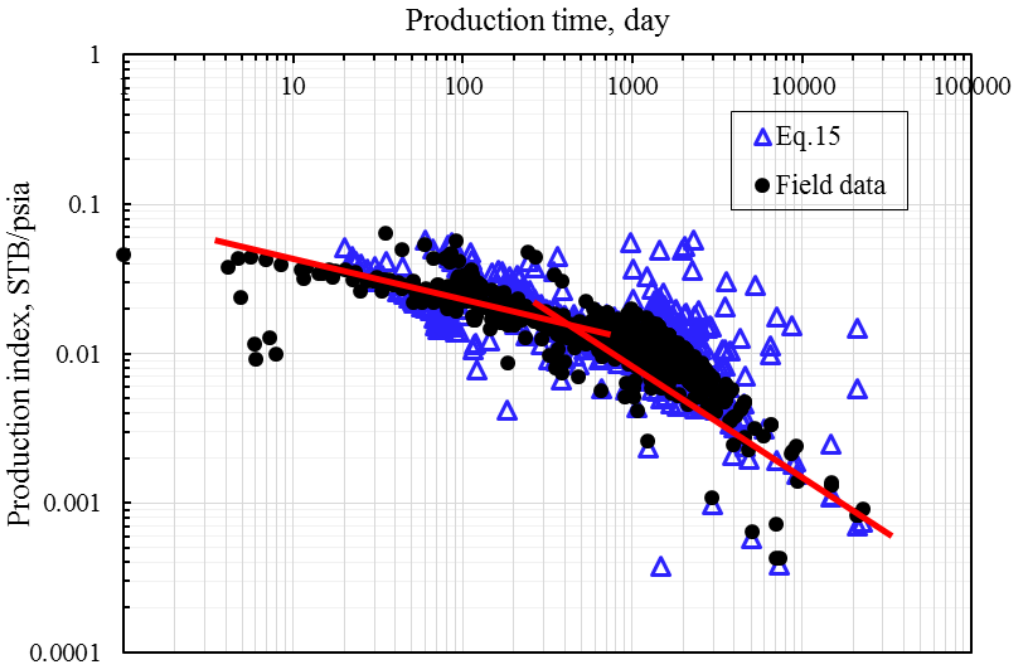

Figure 5.5 Transient-production index using our new empirical equation and field data. The different slope during the early linear-flow and the late compound-linear flow indicates the end of linear flow regime.

To quantify the production fraction from the outer unstimulated matrix, we perform the comparison of cumulative oil production between two cases (Fig. 5.6): Case 1: considering the fluid flow from the outer matrix; and Case 2: no fluid flow within the outer matrix. There is no difference between two cases during the early linear flow, and they become different during the compound-linear flow regime. Fig. 5.6 indicates that the production contribution from the fluid flow from the outer matrix is not substantial but not negligible, i.e., the contribution fraction is almost 3.4% after 10-year depletion production.

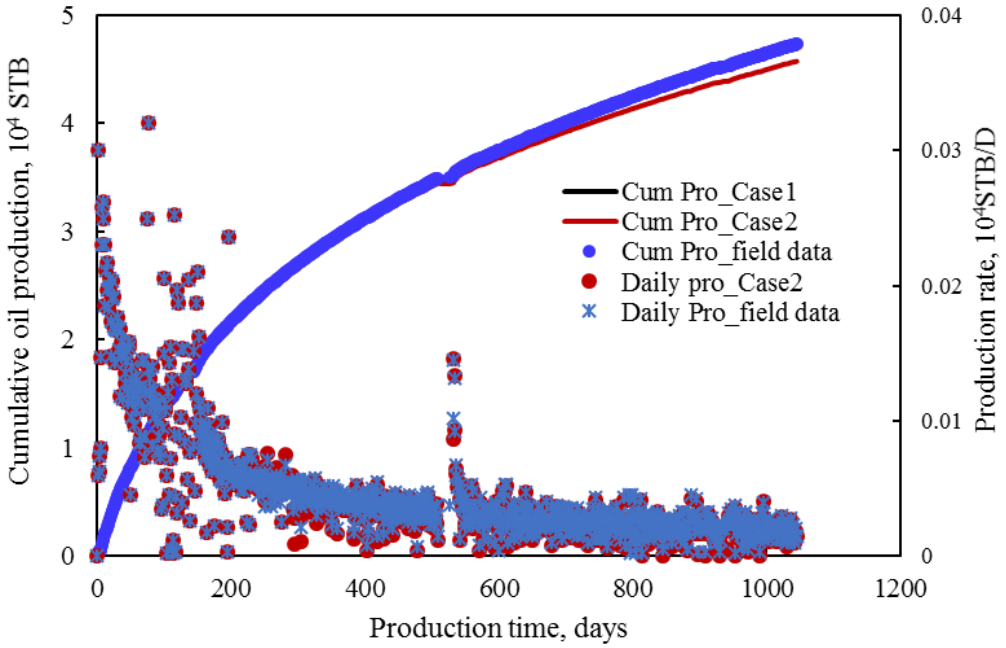

Figure 5.6 Production rate calculated from macroscopic model for two cases and field data. The difference between those two solid lines (black-line and red-line) is the production contribution from the outer matrix

5.2 Production Prediction of MFHW

It is important for the oil companies to have a clear understanding upon the maximum reserves to be produced by the existing wells. Recently, various analytical model has been proposed to match with well production history and make predication as

well, i.e., tri-linear flow model (Ozkan et al. 2009), composite model (Bello and Wattenbarger 2008), multiple-linear flow model (Yuan et al. 2015), composite multi-linear flow coupled with fractal mathematics (Wang et al. 2015). In view of the disadvantages related to analytical models which require the accuracy of input data and simplified assumption, the empirical models are the most widely used forecasting technique in petroleum industry in spite of some errors related to them. As the linear flow assumption in our above integrated production analysis, the modified Duong linear flow model (Eq. 3.25) (Duong 2010 and Joshi 2012) is applied to make predication combined with the above production analysis workflow.

The parameters a and m are calculated using regression analysis by the plot between the left part of Eq.3.25 and the production time, as shown in Fig. 5.7. Followed by, the initial production rate, q_1, can be determined by plotting the flow rates versus *t (a, m)* through Eq.3.26 and Eq.3.27, as shown in Fig. 5.8.

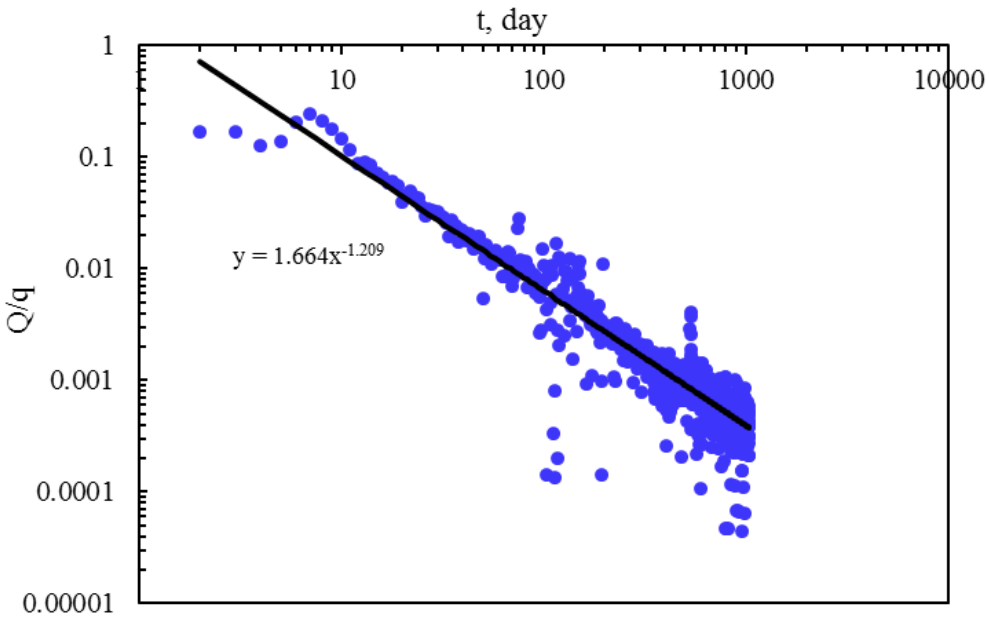

Figure 5.7 Determination of parameter a and m for a MFHW in Niobrara shale oil play

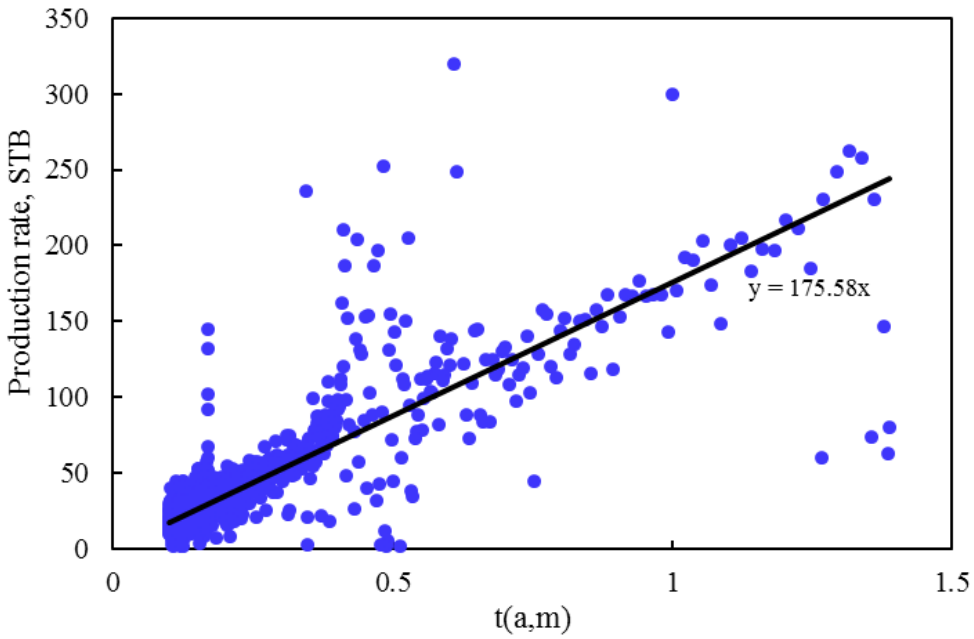

Figure 5.8 Determination of q1 using production data regression of a MFHW in Niobrara shale oil play

Depends on the modified Duong's DCA method, the intercept of regress line in fig. 5.7 is forced to be zero to offset the effect of short-term production history (6-12 months). It has been justified that the setting of q_∞ as zero works better to make predication in most of field cases (Joshi, 2012).

After we get the empirical Duong's model using production history, then we can predict the future performance of MFHW, as shown in Fig. 5.9. in this resesarch, the minimum economic production rate is assumed to be 2 STB/D for the well abandonment condition. We combine the predict production data with the above macroscopic code to evaluate the maximum drainage volume (MDV), associated average reservoir pressure within MDV, and the ultimate recovery factor for this MFHW in this shale oil play, as shown in Table.5.2.

Table 5.2 The estimated and predicted results for a MFHW in Niobrara shale oil play

Stimulated-reservoir volume (SRV), 10^4 ft^3	1960
Average permeability within SRV, mD	0.001
Estimated fracture half-length, ft	263
Maximum drainage volume, (MDV), 10^4 ft^3	2555
Ultimate recovery factor (URF), percentage	8.75
Abandonment average reservoir pressure, pisa	275

5.3 Shale play analyzation

In this section, ten MFHW located in the same shale play will be analyzed, and the result will be compared to find out the general conclusion. The parameters regarded as input are provided in table 5.3. The average pressure, average saturation and dynamic drainage volume are plot in Fig. 5.9, Fig 5.10 and Fig. 5.11 separately. The estimated results are listed in Table 5.4.

Table 5.3 The values of input parameters in Niobrara shale oil play, US

Parameters	Synthetic Case
Initial oil saturation/water saturation	0.74/0.26
Permeability of outer shale matrix, md	0.00001
Reservoir porosity at initial reservoir pressure, decimal	0.075
Water compressibility, psi^{-1}	3.4×10^{-6}
Formation compressibility, psi^{-1}	1×10^{-5}
Oil viscosity at the initial reservoir condition, cp	1.0
Formation Thickness, ft	50
Initial reservoir pressure, psia	7030
Coefficient of oil viscosity	1×10^{-5}
Coefficient of reservoir permeability	4×10^{-4}
Bubble-point pressure, psia	2500
Temperature, F	250
API of oil	45.4
Gas gravity	0.8377
Water density, lb/ft^3	59.3
Well length of MFHW, ft	Well dependent
Number of fracture clusters	Well dependent
Fracture spacing, ft	Well dependent
Half-length of well, ft	Well dependent

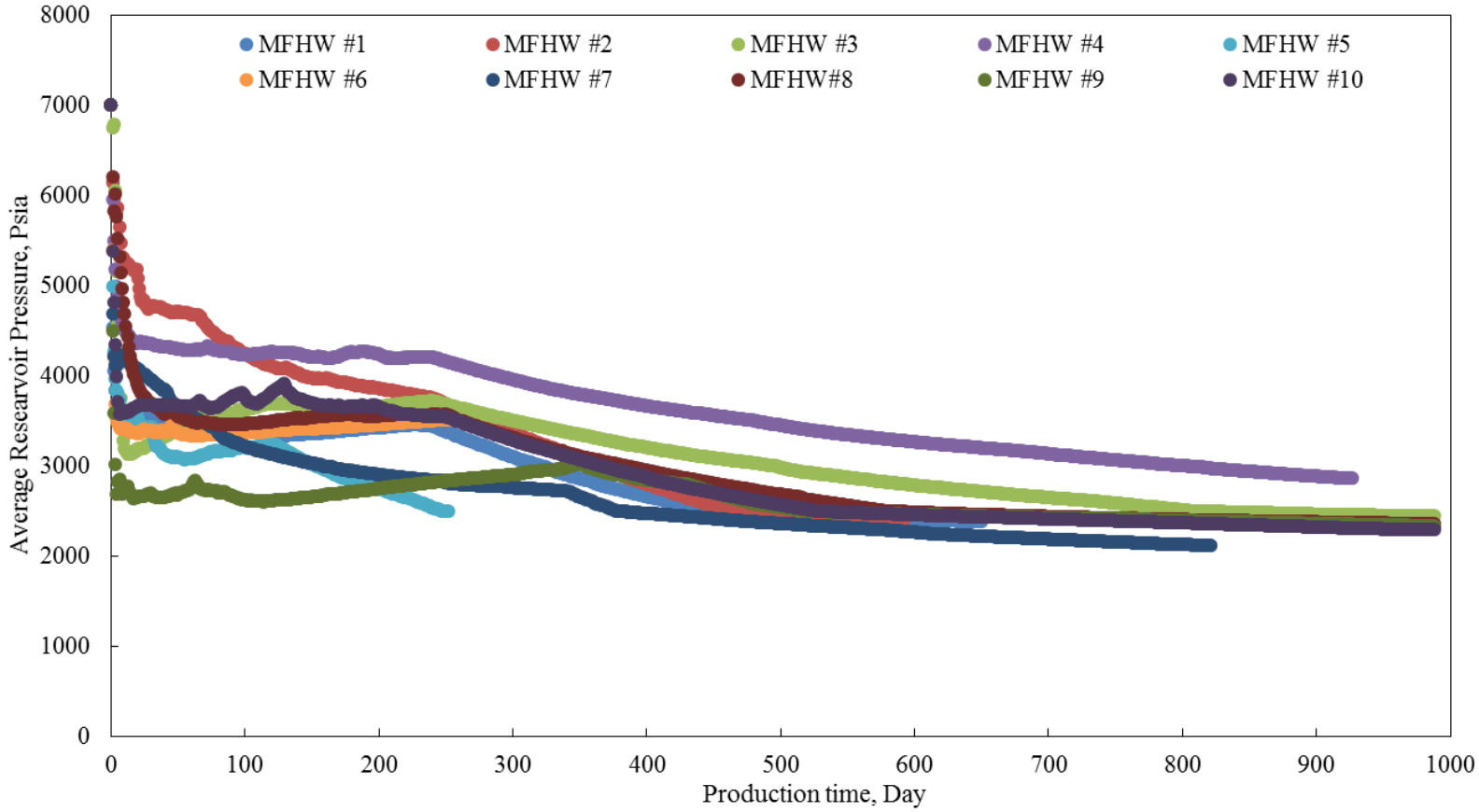

Figure 5.9 Evaluation of average reservoir pressure changing with production time for 10 MFHWs in the same shale oil play

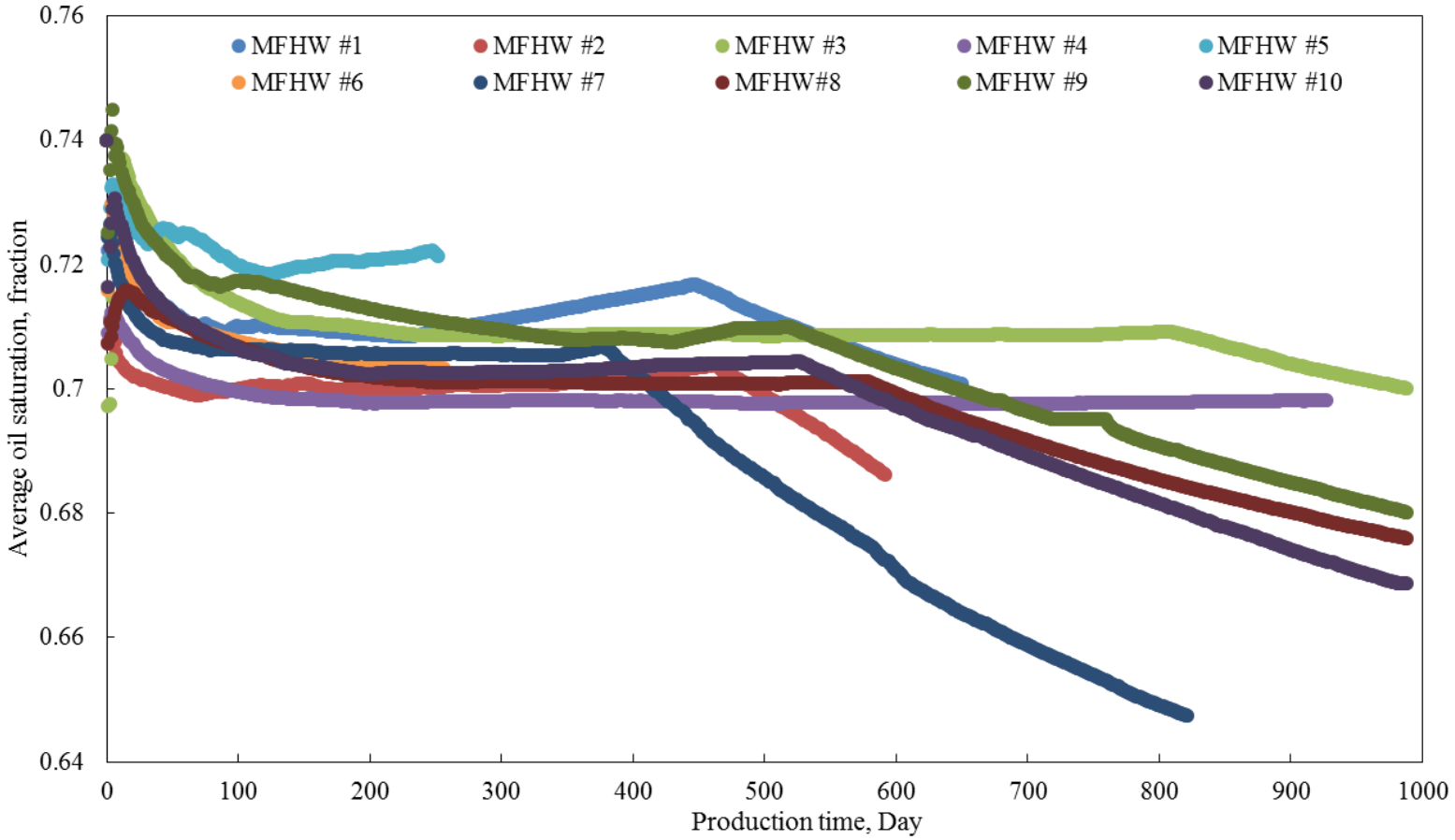

Figure 5.10 Evaluation of average oil saturation changing with production time for 10 MFHWs in the same shale oil play

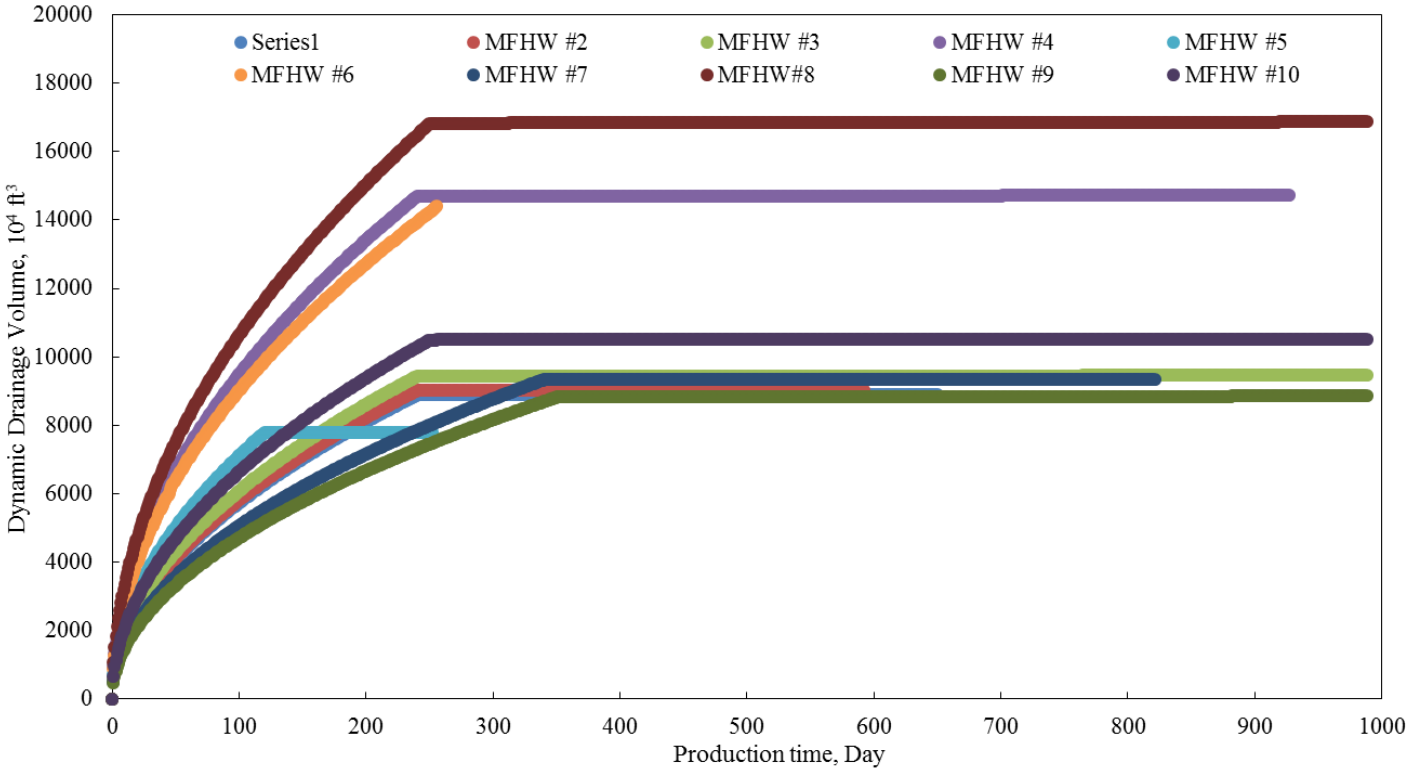

Figure 5.11 Evaluation of Dynamic Drainage Volume (DDV) changing with production time for 10 MFHWs in the same shale oil play

Table 5.4 The estimated and predicted results in Niobrara shale oil play

Parameters	MFHW #1	MFHW #2	MFHW #3	MFHW #4	MFHW #5
Lateral length of horizontal well, ft	4003	4475	4027	6230	3474
Number of fracture cluster, number	48	69	74	157	57
Stimulated-reservoir volume (SRV), 10^4 ft^3	8927	8995	9504	14578	7782
Average permeability within SRV, mD	0.0004	0.0003	0.0002	0.0001	0.0004
Estimated fracture half-length, ft	223	201	236	234	224
Maximum drainage volume, (MDV), 10^4 ft^3	11388	18890	11959	18681	10011
Ultimate recovery factor (URF), percentage	7.21	10.34	7.96	6.39	7.91
Parameters	**MFHW #6**	**MFHW #7**	**MFHW #8**	**MFHW #9**	**MFHW #10**
Lateral length of horizontal well, ft	6400	4000	4380	4152	4914
Number of fracture cluster, number	80	140	74	57	75
Stimulated-reservoir volume (SRV), 10^4 ft^3	11776	9386	9373	8802	11459
Average permeability within SRV, mD	0.0003	0.00006	0.0002	0.0004	0.0004
Estimated fracture half-length, ft	243	247	214	212	233
Maximum drainage volume, (MDV), 10^4 ft^3	17309	18765	19348	11452	14686
Ultimate recovery factor (URF), percentage	9.45	5.87	10.76	9.82	10.25

Inferred from our previous work (Yuan 2016), this paper proposes a new IPR formulation (Eq. 4.17), and derives oil-gas-water multiphase inflow performance relationship (IPR).

In Eq. 4.17, all the variables are pressure-dependent, and that the corresponding pressure is average reservoir pressure within dynamic drainage volume (DDV). This average pressure of 10 wells have been obtained from the above part using macroscopic code. During transient flow regimes in shale reservoirs, the DDV is always dynamically expanding and thereby the average pressure also keeps changing; therefore, this IPR correlation coupled the effects of changing average reservoir pressure can represent well performance during the transient flow regime in shale/tight reservoirs. The comparison of new transient IPR and Vogel IPR for 10 wells are listed in Fig. 5.12(a)-(j). The matching coefficient of a and b for 10 wells keep constant as 0.8 and 1.0, respectively.

To quantify the accuracy of new transient IPR model, we define a cumulative error, which means the cumulative relative difference between the envelop area of different PI curve in Fig.5.12, as shown in Eq. 5.2. The comparison results are presented in Table. 5.5. The comparison results indicate the feasibility and accuracy to apply the new proposed IPR model to predict the well performance in shale oil reservoirs.

$$Error_{\text{model}} = \left| \frac{\sum_{i=2}^{N} J_{i\_\text{field data}} \left(t_{i+1} - t_{i-1}\right) - \sum_{i=2}^{N} J_{i\_\text{model}} \left(t_{i+1} - t_{i-1}\right)}{\sum_{i=2}^{N} J_{i\_\text{field data}} \left(t_{i+1} - t_{i-1}\right)} \right| \times 100\% \quad \text{.....(5.2)}$$

Table 5.5 Cumulative error of IPR results between Vogel model and new model

Well number	Error_Vogel model	Error_New model
MFHW 1#	142%	35%
MFHW 2#	104%	0.8%
MFHW 3#	72%	18%
MFHW 4#	80%	0.2%
MFHW 5#	213%	71%
MFHW 6#	66%	0.6%
MFHW 7#	167%	22%
MFHW 8#	25%	24%
MFHW 9#	42%	25%
MFHW 10#	25%	37%

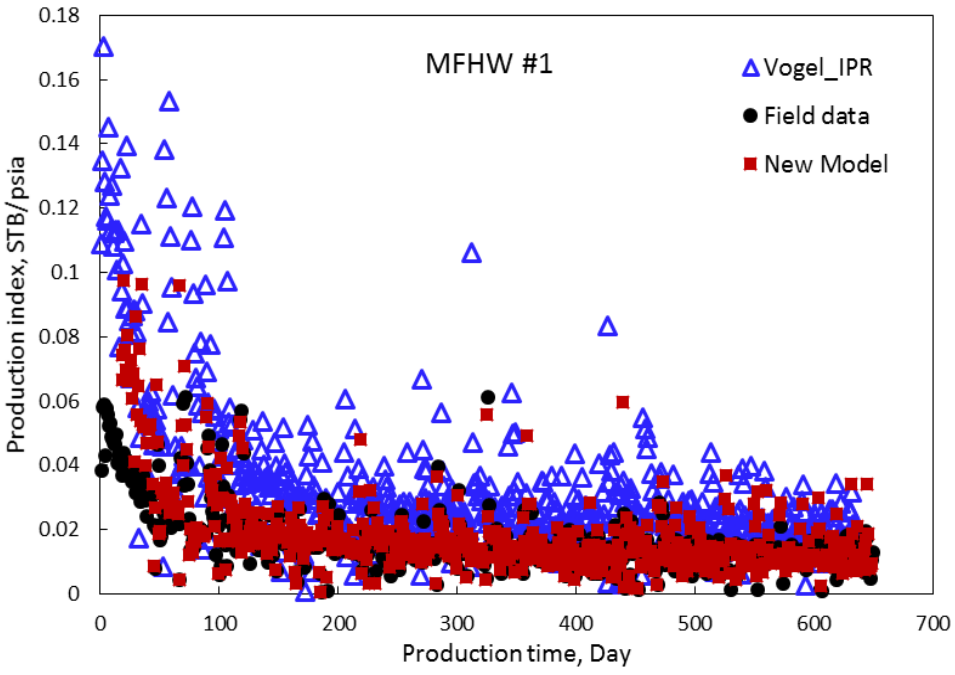

(a)

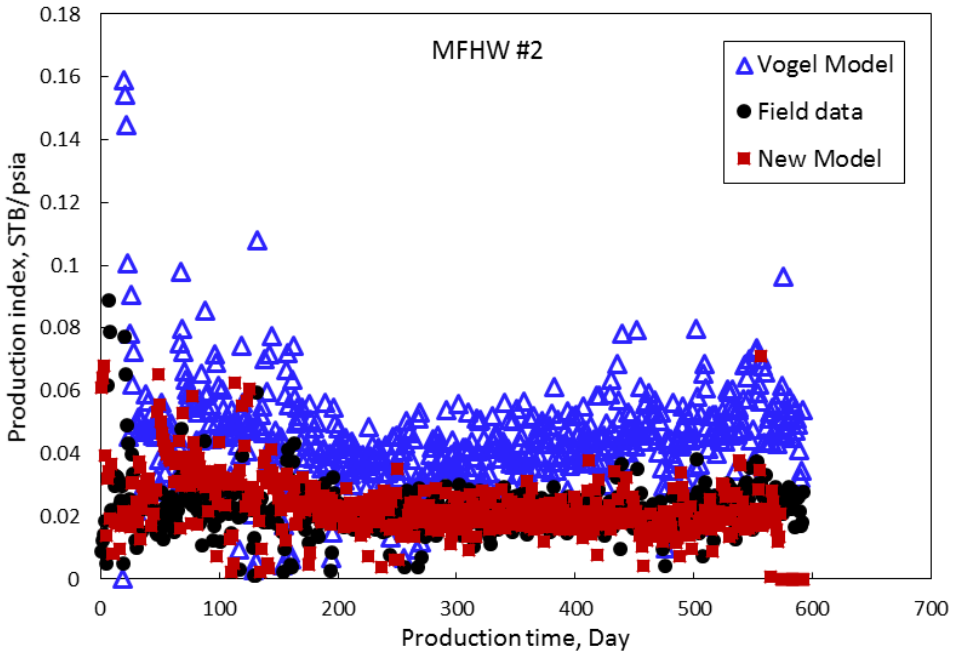
MFHW #2
Vogel Model
Field data
New Model
Production index, STB/psia
Production time, Day
0.18
0.16
0.14
0.12
0.1
0.08
0.06
0.04
0.02
0
0
100
200
300
400
500
600
700

(b)

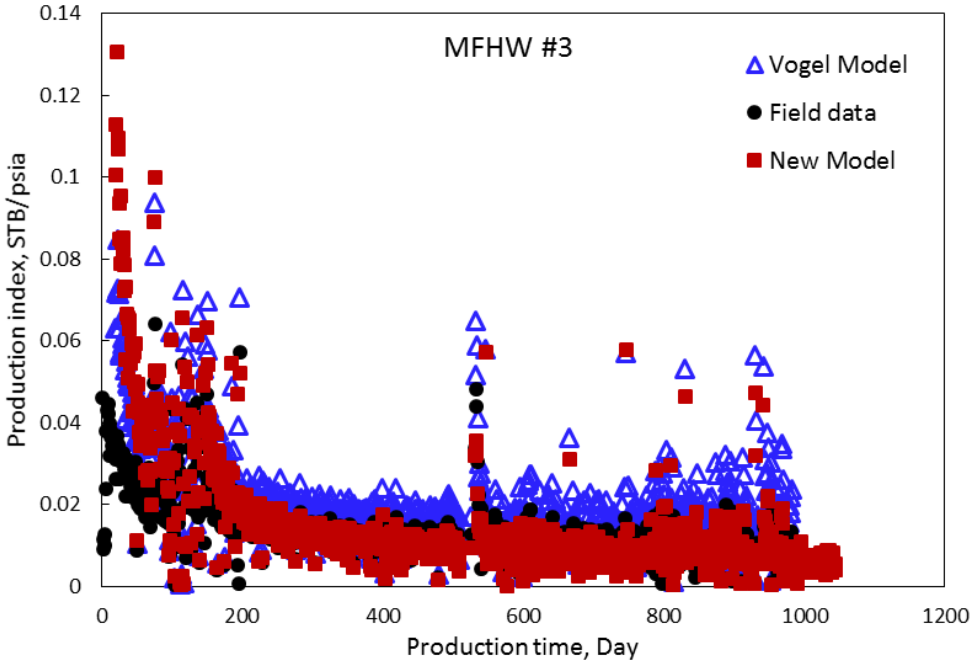
MFHW #3
Vogel Model
Field data
New Model
Production index, STB/psia
Production time, Day
0.14
0.12
0.1
0.08
0.06
0.04
0.02
0
0
200
400
600
800
1000
1200

(c)

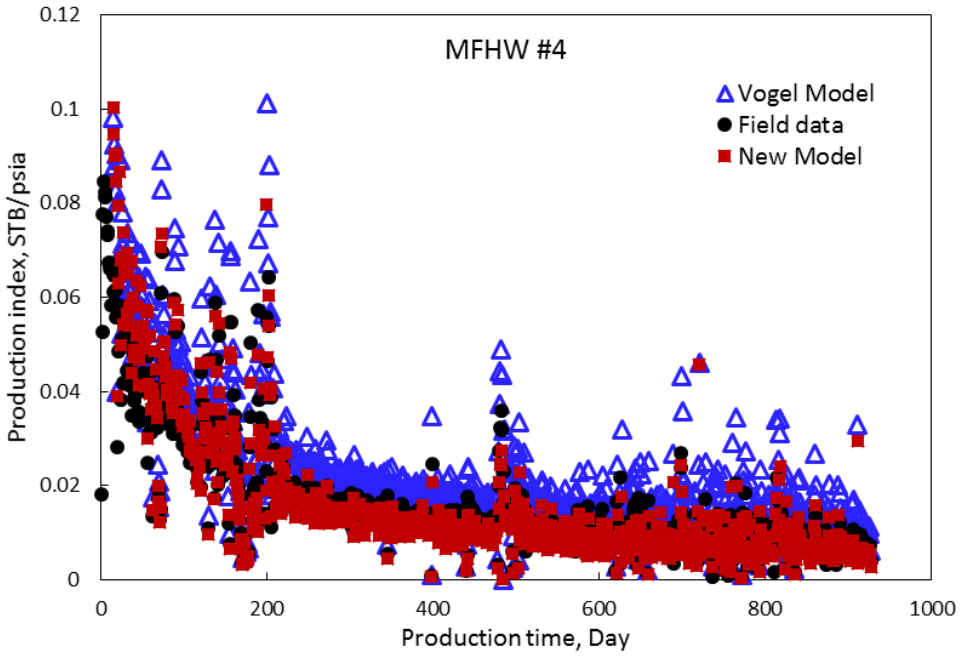
MFHW #4
Vogel Model
Field data
New Model
Production index, STB/psia
Production time, Day
0.12
0.1
0.08
0.06
0.04
0.02
0
0
200
400
600
800
1000

(d)

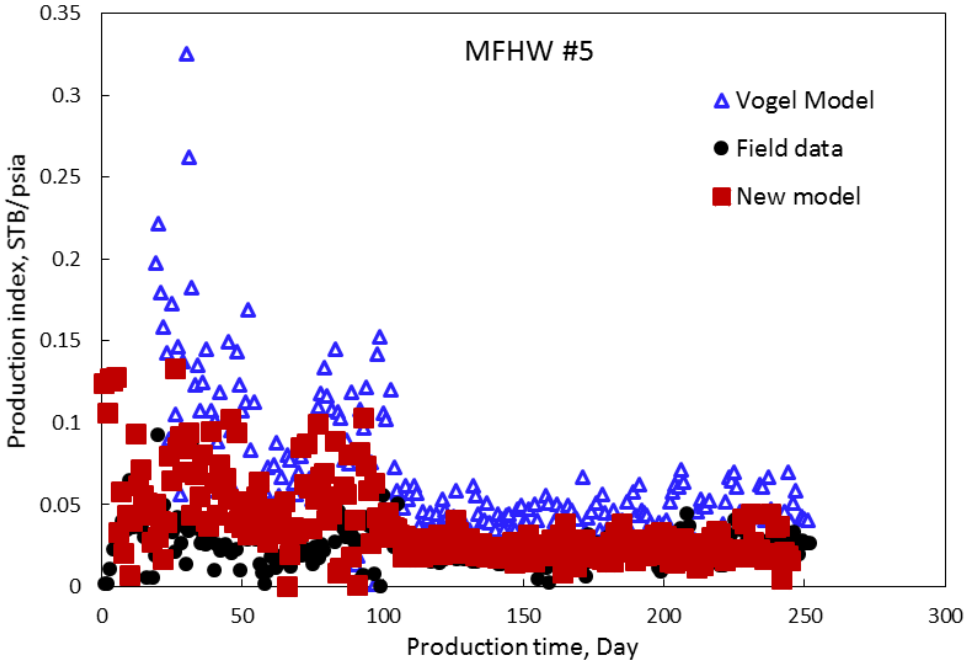
MFHW #5
Vogel Model
Field data
New model
Production index, STB/psia
Production time, Day
0.35
0.3
0.25
0.2
0.15
0.1
0.05
0
0
50
100
150
200
250
300

(e)

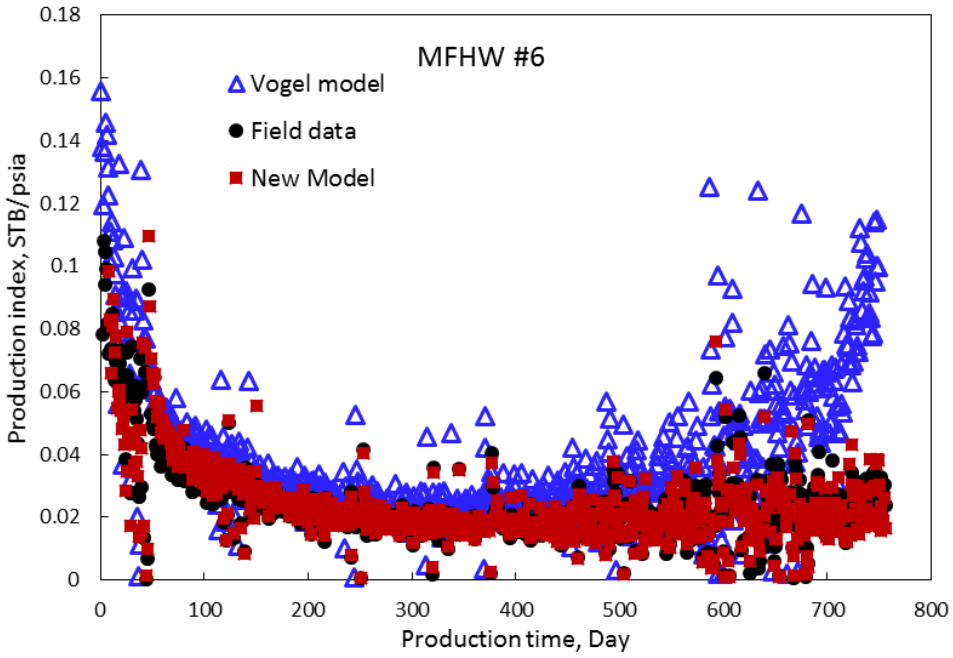
MFHW #6
Vogel model
Field data
New Model
Production index, STB/psia
Production time, Day
0.18
0.16
0.14
0.12
0.1
0.08
0.06
0.04
0.02
0
0
100
200
300
400
500
600
700
800

(f)

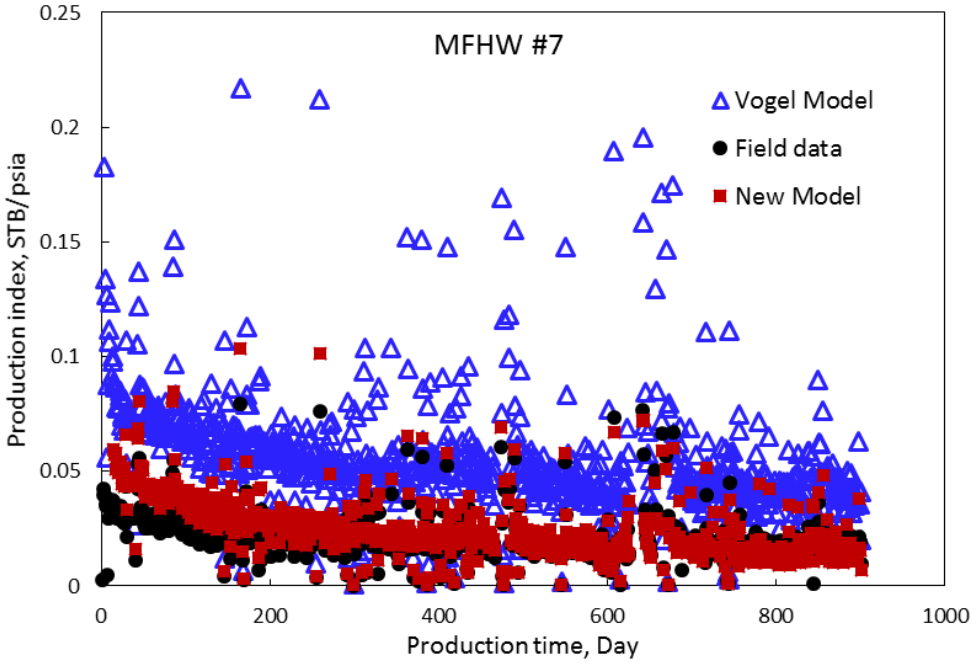
MFHW #7
Vogel Model
Field data
New Model
Production index, STB/psia
Production time, Day
0.25
0.2
0.15
0.1
0.05
0
0
200
400
600
800
1000

(g)

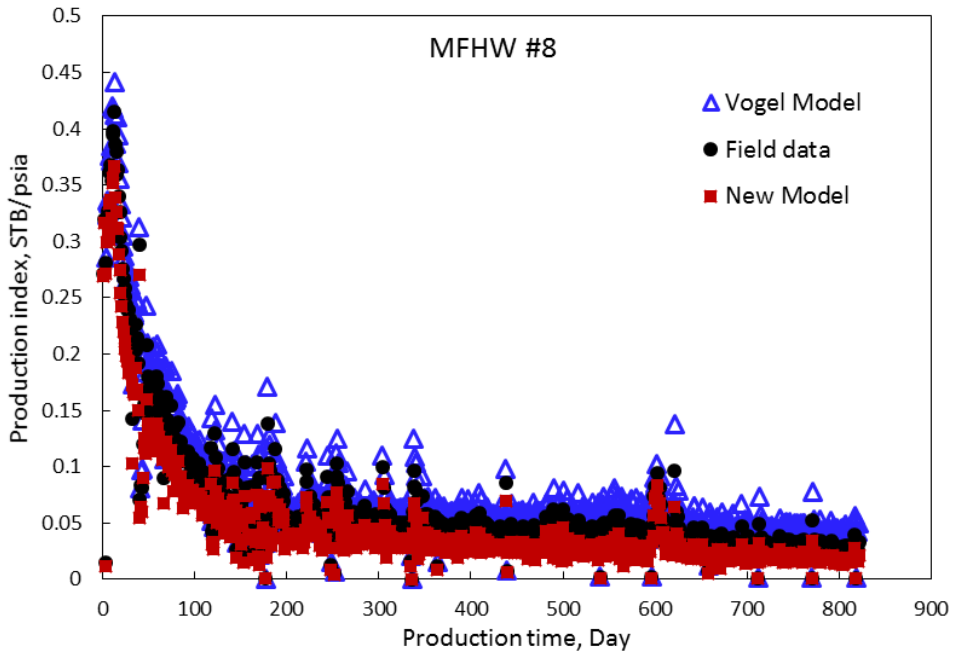
MFHW #8
Vogel Model
Field data
New Model
Production index, STB/psia
Production time, Day
0.5
0.45
0.4
0.35
0.3
0.25
0.2
0.15
0.1
0.05
0
0
100
200
300
400
500
600
700
800
900

(h)

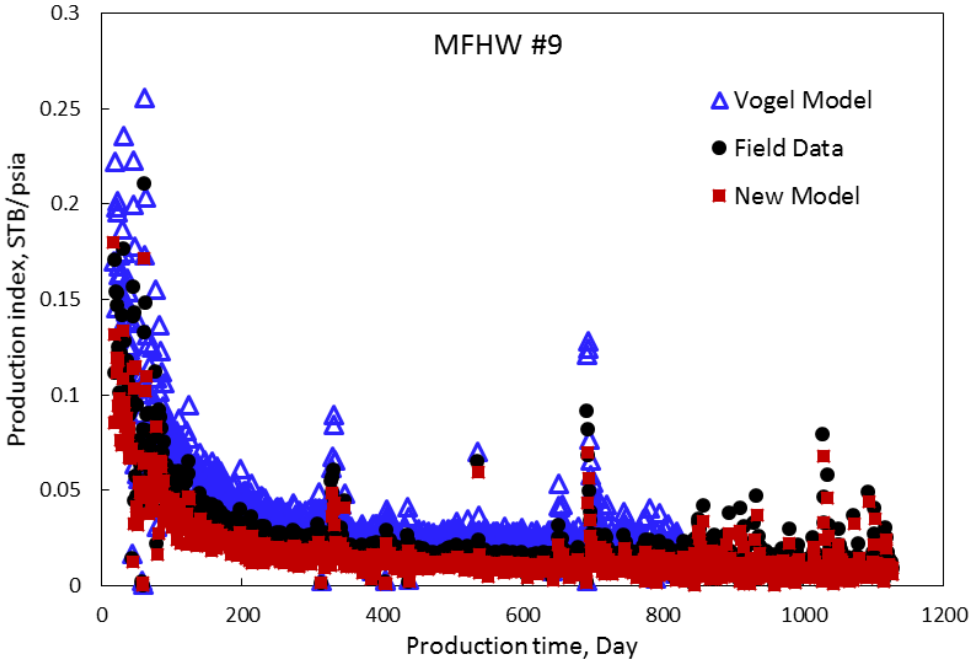
MFHW #9
Vogel Model
Field Data
New Model
Production index, STB/psia
Production time, Day
0.3
0.25
0.2
0.15
0.1
0.05
0
0
200
400
600
800
1000
1200

(i)

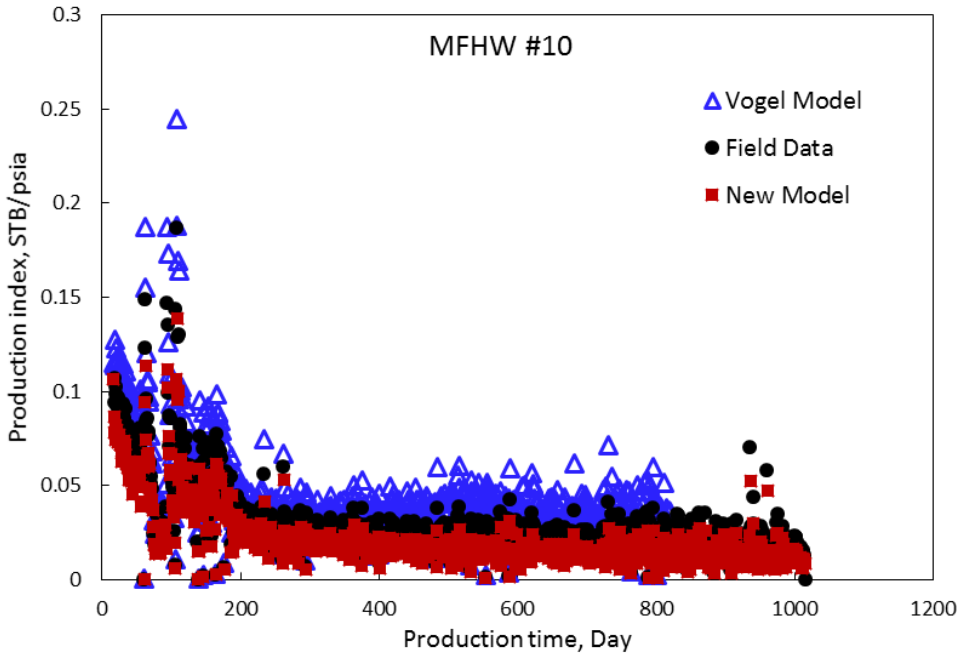

(j)

Figure 5.12 Comparison results of Vogel IPR, new IPR model and actual field data

Another objective of this paper is to determine the optimal fracture design (fracture spacing) and well spacing, after we have finished the estimate of fracture and reservoir properties using rate-transient analysis (Yuan 2016). To eliminate the effects of different horizontal well length on well performance, the well length-normalized EUR is the ultimate recovery of MFHW divided by the length of horizontal section, which represents the contribution of fracture spacing alone. Fig.5.13 indicates the optimal fracture spacing for the multistage fractured horizontal well in Niobrara shale oil, approximately 60-70 ft. In view of the optimal fracture case, based on the design of bottom-hole flowing pressure, the oil production rate can be read out from the IPR curves under the condition of different average reservoir pressure. The correlation between production rate calculated from new IPR model and actual field production data is shown as Fig.5.14.

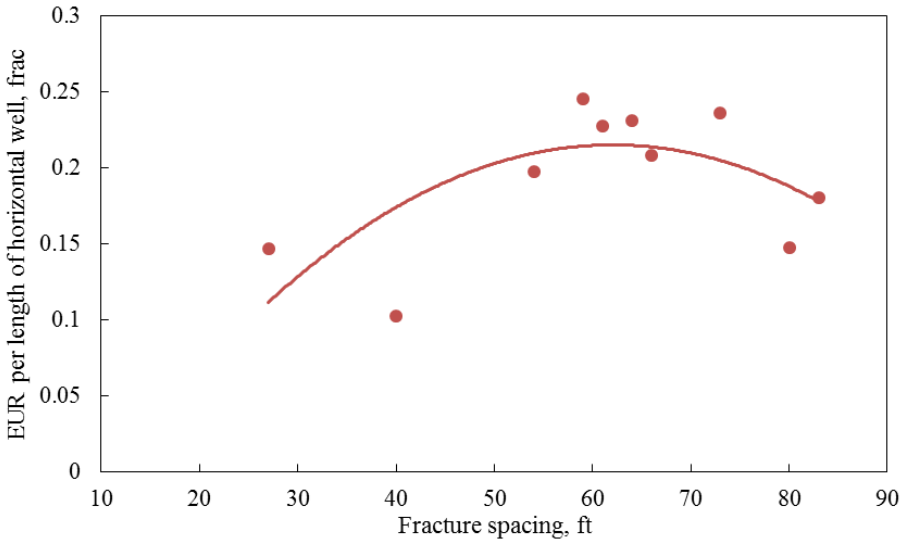

Figure 5.13 Relation between fracture spacing and horizontal well length normalized EUR of multistage fractured horizontal well

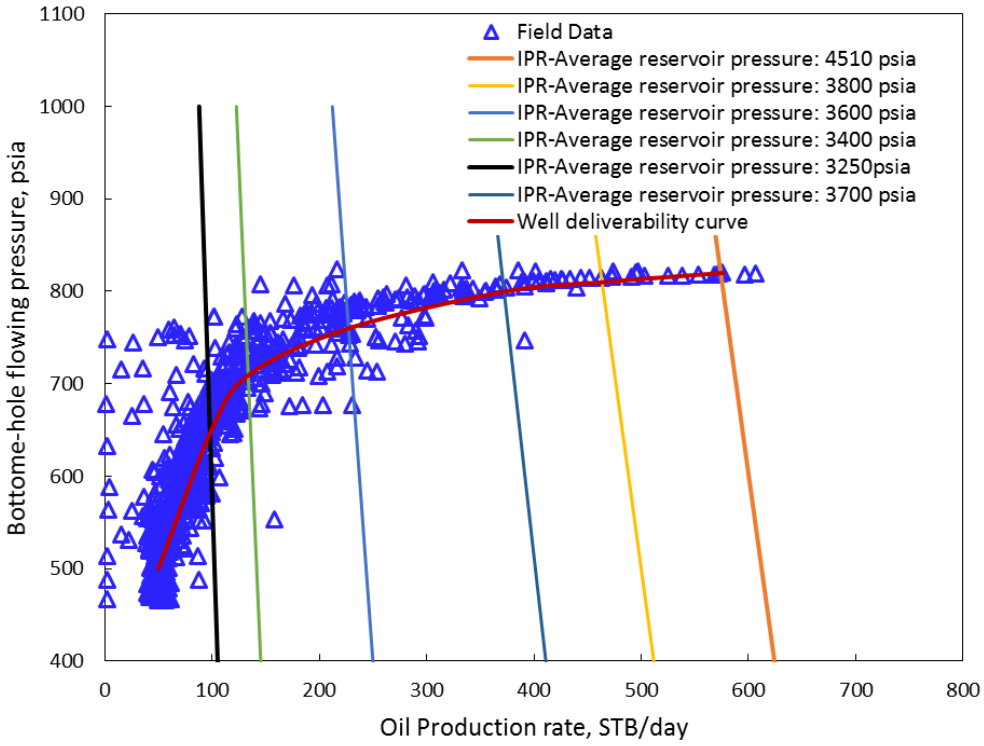

Figure 5.14 The comparison between production rates derived from new IPR model and actual field data for the optimal fracture design

Chapter 6: Conclusion

(1) The analytical solution of dynamic drainage volume (DDV) is proposed, including the fluid flow contribution of both inner reservoir and outer reservoir.

(2) The novel equation of DDV can be used to evaluate the performance of multi-stage fractured horizontal well (MFHW). There is a linear relation between DDV and square-root of time for both transient linear and compound linear flow regimes.

(3) There are various important factors controlling the advancement of DDV, i.e., fracture spacing, fracture length, the diffusivities of both inner reservoirs (SRV) and outer reservoirs (unstimulated matrix).

(4) The effects of stress-dependent and pressure-dependent fluid properties on production analysis are incorporated by a pressure-dependent correction factor. The half-length of primary fracture and diffusivity within SRV are also evaluated using an iterative algorithm combined RNP, square-root-of-time, and transient production index together.

(5) Using the integrated production analysis, the average reservoir pressure, recovery factor (RF) and phase saturation (oil/gas/water) are achieved from production history; ultimate drainage volume (estimated as ultimate recovery, EUR) is also predicted at abandonment condition.

(6) Moreover, the contributions of both unstimulated-reservoir matrix and stimulated-reservoir volume (SRV) are quantified with changing time, respectively. The contribution from the outer matrix is small but not negligible.

(7) New IPR correlation can better match with production history and provide us graphic approach to predict new well performance.

(8) By comparing the different EUR normalized by horizontal well length for the difference cases of fracture spacing, we determine the optimal fracture spacing for this reservoir approximated as 60-70 ft.

(9) Well deliverability curve (bottom-hole pressure vs. oil production rates) of the optimal fracture design case is achieved by using new IPR model.

Nomenclature

C_{RD} = dimensionless reservoir conductivity

c_{tO} = total outer reservoir compressibility, psi^{-1}

c_{tI} = total inner reservoir compressibility, psi^{-1}

c_f = formation compressibility, psi^{-1}

c_μ = viscosity modulus

γ_k = permeability modulus

h = reservoir thickness, ft

k_I = permeability of the inner reservoir, md

k_O = permeability of the outer reservoir, md

p = pressure, psi

p_i = initial pressure, psi

p_b = bubble point pressure, psi

p_{wf} = well flow pressure, psi

q = production rate, STB/day

s = Laplace parameter

s_o = Parameter defined in trilinear flow model

t = time, days

t_D = dimensionless time

x = x coordinate, ft

x_D = *dimensionless x coordinate, ft*

x_f = hydraulic fracture half-length, ft

y = y coordinate, ft

y_e = half of distance between two hydraulic fractures, ft

y_D = dimensionless y coordinate, ft

y_{eD} = *dimensionless half of fracture spacing*

α = Parameter defined in trilinear flow model

η_I = inner-reservoir diffusivity, ft^2/hr

η_O = outer-reservoir diffusivity, ft^2/hr

η_{OD} = outer-reservoir diffusivity ratio, ft^2/hr

μ = fluid viscosity, cp

ϕ_I = inner- reservoir porosity, fraction

ϕ_O = outer- reservoir porosity, fraction

J = productivity index, bbl/psi

B_o = oil formation volume factor, bbl/STB

B_w = water formation volume factor, bbl/STB

RNP = rate normalized pressure, psi/bbl

t_e = material balance time

t_{ma} =material balance pseudotime

f_{cp} = correction factor

m(p) = pseudopressure

S_o = oil saturation, fraction

S_g = gas saturation, fraction

S_w = water saturation, fraction

S_{oi} = initial oil saturation, fraction

S_{gi} = initial gas saturation, fraction

S_{wi} = initial water saturation, fraction

k_{ro} = relative permeability of oil

References

Aguilera, R., 1987. Well Test Analysis of Naturally Fractured Reservoirs. SPE Formation Evaluation, 2(03), 239-252.

Aguilera, R., 2006. Radius And Linear Distance of Investigation and Interconnected Pore Volume in Naturally Fractured Reservoirs. Journal of Canadian Petroleum Technology, 45(12).

Anderson, D., and Mattar, L. 2007. An Improved Pseudo-Time for Gas Reservoirs With Significant Transient Flow, Journal of Canadian Petroleum Techonology 45(07): 46-54. PETSOC-07-07-05.

Apaydin, O.G., Ozkan, E., Raghavan, R. 2012. Effect of Discontinuous Microfractures on Ultratight Matrix Permeability of a Dual-porosity Medium. SPE Reserv. Eval. Eng 15 (4), 473-485.

B. C. Craft and M. Hawkins. 1991. Applied Petroleum Reservoir Engineering. Prentice Hall Inc. Upper Saddle River, NJ. USA.

Behmanesh, H., Hamdi, H. and Clarkson, C.R. 2015. Production Data Analysis of Tight Gas Condensate Reservoirs. Journal of Natural Gas Science and Engineering, 22, 22-34.

Behmanesh, H., Clarkson, C.R., Tabatabaie, S.H. and Heidari Sureshjani, M. 2015. Impact of Distance-of-Investigation Calculations on Rate-Transient Analysis of Unconventional Gas and Light-Oil Reservoirs: New Formulations for Linear Flow. Journal of Canadian Petroleum Technology.

Brown, M. L., Ozkan, E., Raghavan, R. S., & Kazemi, H. 2009. Practical Solutions for Pressure Transient Responses of Fractured Horizontal Wells in Unconventional Reservoirs. Society of Petroleum Engineers.

Brown, M., Ozkan, E., Raghavan, R., Kazemi, H. 2011. Practical Solutions for Pressuretransient Responses of Fractured Horizontal Wells in Unconventional Shale Reservoirs. Society of Petroleum Engineers Reservoir Evaluation & Engineering 14 (6), 663–676.

Carslaw, H. S., and Jaeger, J. C. 1959. Conduction of Heat in Solids. Second ed. Oxford University Press, Oxford.

Cheng, Y., W. J. Lee and D. A. McVay, 2009. A New Approach for Reliable Estimation of Hydraulic Fracture Properties Using Elliptical Flow Data in Tight Gas Wells. SPEJ 12(02): 9.

Cipolla, C. L., E. P. Lolon, J. C. Erdle and B. Rubin, 2010. Reservoir Modeling in Shale-Gas Reservoirs. SPE Reservoir Evaluation & Engineering 13(04): 16.

Clarkson, C. R. and J. J. Beierle, 2011. Integration of microseismic and other post-fracture surveillance with production analysis: A tight gas study. Journal of Natural Gas Science and Engineering 3(2): 382-401.

Clarkson, C.R. 2013. Production Data Analysis of Unconventional Gas Wells: Review of Theory and Best Practices. Int. J. Coal Geol. 109-110 (0), 101-146.

Dong Z., Holditch S. A., McVay D.A., Resource Evaluation for Shale Gas Reservoirs. SPE Econ Manage 2013: 5(1): 5-16. SPE-15206-PA.

Duong, A.N. 2010. An Unconventional Rate Decline Approach for Tight and Fracture-Dominated Gas Wells. Paper presented at the Canadian Unconventional Resources and International Petroleum Conference, Calgary, Alberta, Canada. Society of Petroleum Engineers SPE-137748-MS.

F. Medeiros, B. Kurtoglu, E. Ozkan and H. Kazami, 2010. Analysis of Production Data from Hydraulically Fractured Horizontal Wells in Shale Reservoirs. SPE Reservoir Evaluation & Engineering 13(03): 559-570.

Javadpour, F., 2009. "Nanopores and Apparent Permeability of Gas Flow in Mudrocks (Shales and Siltstone)." Journal of Canadian Petroleum Technology 48(08): 16-21.

Joshi, K. J., 2012. Comparison of Various Deterministic Forecasting Techniques in Shale Gas Reservoirs with Emphasis on The Duong Method. Texas A& M University.

Jones, P., 1962. Reservoir Limit Test on Gas Wells; Journal of Petroleum Technology, pp. 217-223.

King, G. E., 2010. Thirty Years of Gas Shale Fracturing: What Have We Learned? SPE Annual Technical Conference and Exhibition. Florence, Italy, Society of Petroleum Engineers.

Kuchuk, F.J., 2009, January. Radius of Investigation for Reserve Estimation from Pressure Transient Well Tests. Paper SPE-120515 presented at SPE Middle East Oil and Gas Show and Conference. Society of Petroleum Engineers.

Lee, S.-T., & Brockenbrough, J. R., 1986. A New Approximate Analytic Solution for Finite-Conductivity Vertical Fractures. Society of Petroleum Engineers. doi:10.2118/12013-PA

Lee, J., Rollins, J.B., Spivey, J.P., 2003. Pressure Transient Testing. Richardson, Texas, Society of Petroleum Engineers.

Meyer, B.R., Bazan, L.W., Jacot, R.H., et al. 2010. Optimization of Multiple Transverse Hydraulic Fractures in Horizontal Wellbores. Paper SPE-131732 Presented at the SPE Unconventional Gas Conference, Pittsburgh, Pennsylvania, USA.

Moghanloo, R. G., Yuan, B., Ingrahama, N., Kramf, E., Arrowooda, J., and Dadmohammadi, Y., 2015, “Applying Macroscopic Material Balance to Evaluate Interplay Between Dynamic Drainage Volume and Well Performance in Tight Formations,” J. Nat. Gas Sci. Eng., 27(2), pp. 446–478.

Moghanloo, R. G., & Hosseinipour, S. S., 2014. Mechanistic Modeling of Fluid Flow in Shale. Society of Petroleum Engineers. doi:10.15530/urtec-2014-1921547.

Nobakht, M., & Clarkson, C. R., 2012. A New Analytical Method for Analyzing Linear Flow in Tight/Shale Gas Reservoirs: Constant-Flowing-Pressure Boundary Condition. SPE Reservoir Evaluation & Engineering, 15(03), 370-384.

Nobakht, M., 2014. New and Improved Methods for Performing Rate-transient Analysis of Tight/Shale Gas Reservoirs. PhD thesis. University of Calgary, Department of Chemical and Petroleum Engineering, Calgary, Alberta, Canada.

Ozkan, E., Brown, M.L., Raghavan, R.S. and Kazemi, H., 2009, January. Comparison of Fractured Horizontal-well Performance in Conventional and Unconventional Reservoirs. Paper SPE-121290 presented at SPE Western Regional Meeting, 24-26 March, San Jose, California

Osholake, T., J. Yilin Wang, and T. Ertekin, 2012. Factors Affecting Hydraulically Fractured Well Performance in the Marcellus Shale Gas Reservoirs. Journal of Energy Resources Technology. 135(1): p. 013402-013402.

Qanbari, F. and Clarkson, C.R., 2013. A new method for production data analysis of tight and shale gas reservoirs during transient linear flow period. Journal of Natural Gas Science and Engineering, 14, pp.55-65.

Rouzbeh Ghanbarnezhad Moghanloo, Bin Yuan and N., 2015. Applying Macroscopic Material Balance to Evaluate Dynamic Drainage Volume and Performance Prediction of Shale Oil/Gas Wells. Journal of Natural Gas Science and Engineering, Vol. 27, Part 2, November 2015, Pages 466–478.

Seidle, J. P., 1999. Coal Well Decline Behavior and Drainage Areas: Theory and Practice. SPE Gas Technology Symposium. Calgary, Alberta, Canada, Society of Petroleum Engineers.

Sobbi, F. A., & Badakhshan, A., 1996. Radius of Investigation for Well Tests in Dual Porosity Reservoirs. Journal of Canadian Petroleum Technology, 35(6), 49-54.

Song, B., Economides, M.J., Ehlig-Economides, C., 2011. Design of Multiple Transverse Fracture Horizontal Wells in Shale Gas. Paper 140555 Presented at the SPE Hydraulic Fracture Technology Conference, The Woodlands, Texas.

Stalgorova, E., Mattar, L., 2012. Analytical Model for History Matching and Forecasting Production in Multifrac Composite Systems. In: SPE Paper 162516 Presented at SPE Canadian Unconventional Resource Conference, Calgary, Alberta, Canada.

Stehfest, H., 1970. Algorithm 368: Numerical Inversion of Laplace Transforms [D]. Communications of the ACM, 13(1), 47-49.

Sun, J., Huang, C. K., Schechter, D., 2015. Sensitivity Analysis of Unstructured Meshing Parameters on Production Forecast of Hydraulically Fractured Horizontal Wells. Presented at the Abu Dhabi International Petroleum Exhibition and Conference, Abu Dhabi, UAE, 9-12 November. SPE-177480-MS.

Swami, V. and A. Settari, 2012. A Pore Scale Gas Flow Model for Shale Gas Reservoir. SPE Americas Unconventional Resources Conference. Pittsburgh, Pennsylvania USA, Society of Petroleum Engineers.

Tek, M. R., Grove, M. L., and Poettman, F. H., 1957 Method for Predicting the Back Pressure Behavior of Low Permeability Natural Gas Wells; Trans. AIME, pp. 210-302.

Valko, P. P. and W. J. Lee., 2010. A Better Way To Forecast Production From Unconventional Gas Wells. SPE Annual Technical Conference and Exhibition. Florence, Italy, Society of Petroleum Engineers.

Van Everdingen, A. F., and Hurst, W., 1949. The Application of Laplace Transformation to Flow Problems in Reservoirs. Petroleum Transactions, *AIME* **186**: 305-324. SPE 949305-G.

Van Poollen, H.K. "Radius of Investigation and Stabilization Time Equations." Oil Gas J.(1964)63(51), 71-75

Wattenbarger, R. A., El-Banbi, A. H., Villegas, M. E., & Maggard, J. B., 1998. Production Analysis of Linear Flow Into Fractured Tight Gas Wells. Paper SPE-39931 presented at SPE Rocky Mountain Regional/Low Permeability Reservoirs Symposium and Exhibition, Denver, Colorado.

Wang, L. and X. Wang, 2013. Type Curves Analysis for Asymmetrically Fractured Wells. Journal of Energy Resources Technology. 136(2): p. 023101-023101.

Xiaoliang Zhao, Z. Rui, X. Liao, R. Zhang, 2015. The Qualitative and Quantitative Fracture Evaluation Methodology in Shale Gas Reservoir. Journal of natural gas science and engineering, 27, 486-495.

Yin, J., H.-Y. Park, A. Datta-Gupta, M. J. King and M. K. Choudhary, 2011. "A hierarchical streamline-assisted history matching approach with global and local parameter updates." Journal of Petroleum Science and Engineering 80(1): 116-130.

Yuan, B., Zheng, D., and Moghaloo, R. G., 2016. Integrated Production Analysis Using the Concept of Dynamic Drainage Volume: Modelling, Simulation and Field Applications. SPE Asia Pacific Hydraulic Fracturing Conference. 24-26 August, Beijing, China.

Yuan, B., Moghanloo, R. G., Wang, K., Zheng, D., and Li, J., 2016, October 25. An Integrated Approach for Fracturing Evaluation and Optimization using Rate-transient Analysis and Dynamic Drainage Volume. Society of Petroleum Engineers. doi:10.2118/182244-MS

Yuan, B., Moghanloo, R. G., & Zheng, D. 2016, June 1. Analytical Evaluation of Nanoparticle Application To Mitigate Fines Migration in Porous Media. Society of Petroleum Engineers. doi:10.2118/174192-PA

Yuan B., Wood D.A and W. Yu. 2015. Stimulation and Hydraulic Fracturing Technology in Natural Gas Reservoirs: Theory and Case Study (2012-2015), Journal of Natural Gas Science and Engineering, Vol. 26, September 2015, Pages 1414-1421.

Yuan B., Wood, D. A. 2015. Production Analysis and Performance Forecasting for Natural Gas Reservoirs: Theory and Practice (2011-2015), Journal of Natural Gas Science and Engineering, Vol. 26, September 2015, Pages 1433-1438.

Yuan, B., Moghanloo, R. G., & Zheng, D. 2016, September 26. Enhanced Oil Recovery by Combined Nanofluid and Low Salinity Water Flooding in Multi-Layer Heterogeneous Reservoirs. Society of Petroleum Engineers. doi:10.2118/181392-MS

Yuan B., Y. Su, and R. G. Moghanloo et al. 2015. A New Analytical Multi-Linear Solution for Gas Flow toward Fractured Horizontal Well with Different Fracture Intensity. Journal of Natural Gas Science and Engineering, Vol.23, Pages 227–238.

Yuan B., R. G. Moghanloo, and Emad Shariff et al. 2016. Integrated Investigation of Dynamic Drainage Volume (DDV) and Inflow Performance Relationship (Transient IPR) to Optimize Multi-stage Fractured Horizontal Wells in Shale Oil. Journal of Energy Resource Technology, 138(5).

Yuan, B., Moghanloo, R. G., & Zheng, D. 2016, March 22. Analytical Modeling of Nanofluid Injection to Improve the Performance of Low Salinity Water Flooding. Offshore Technology Conference. doi:10.4043/26363-MS

Zhao, X., Rui, Z., Liao, X. and Zhang, R., 2015. A Simulation Method for Modified Isochronal Well Testing to Determine Shale Gas Well Productivity. Journal of Natural Gas Science and Engineering, 27, pp.479-485.

Zhao, Y. L., Zhang, L.-H., Luo, J. X., et al., 2014. Performance of Fractured Horizontal Well with Stimulated Reservoir Volume in Unconventional Gas Reservoir. Journal of Hydrology. 512, 447-456.

Zheng, D., Moghaloo, R. G., and Yuan, B., 2016. Modeling Dynamic Drainage Volume for Multi-Stage Fractured Wells in Composite Shale Systems: New Analytical Solution for Transient Linear Flow. SPE Asia Pacific Hydraulic Fracturing Conference. 24-26 August, Beijing, China.